Acta Astronautica 153 (2018) 311–326

Contents lists available at ScienceDirect

Acta Astronautica

journal homepage: www.elsevier.com/locate/actaastro

Continuous maneuvers for spacecraft formation flying reconfiguration using relative orbit elements

G. Di Mauro [a,*], R. Bevilacqua [a,**], D. Spiller [b], J. Sullivan [c], S. D'Amico [c]

[a] Department of Mechanical and Aerospace Engineering, ADAMUS Laboratory, University of Florida, 939 Sweetwater Dr., Gainesville, FL 32611 – 6250, USA
[b] Department of Mechanical and Aerospace Engineering, Sapienza University of Rome, via Eudossiana 18, 00184, Italy
[c] Department of Aeronautics and Astronautics Engineering, Stanford Space Rendezvous Lab, Stanford University, 496 Lomita Mall, Stanford, CA 94305-4035, USA

ARTICLE INFO

Keywords:
Spacecraft formation flying reconfiguration
Relative orbit elements
Relative motion control

ABSTRACT

This paper presents the solutions to the spacecraft relative trajectory reconfiguration problem when a continuous thrust profile is used, and the reference orbit is circular. Given a piecewise continuous thrust profile, the proposed approach enables the computation of the control solution by inverting the linearized equations of relative motion parameterized using the mean relative orbit elements. The use of mean relative orbit elements facilitates the inclusion of the Earth's oblateness effects and offers an immediate insight into the relative motion geometry. Several reconfiguration maneuvers are presented to show the effectiveness of the obtained control scheme.

1. Introduction

Spacecraft formation flying concepts have become a topic of interest in recent years given the associated benefits in terms of cost, mission flexibility/robustness, and enhanced performance [1,2] Replacing a complex, monolithic spacecraft with an array of simpler and highly coordinated satellites increases the performance of interferometric instruments through the aperture synthesis. The configuration of formations can also be adjusted to compensate for malfunctioning vehicles without forcing a mission abort or be reconfigured to accomplish new tasks.

Among the various technical challenges involved in spacecraft formation flying, the reconfiguration problem represents a key aspect that has been intensively studied over the last years [2] Formation reconfiguration pertains to the achievement of a specific relative orbit in a defined time interval given an initial formation configuration. So far, many methods have been proposed to solve the aforementioned problem, ranging from impulsive to continuous control techniques. Impulsive strategies have been widely investigated since they provide a closed-form solution to the relative motion control problem. Such solutions are generally based on 1) the use of the Gauss variational equations (GVE) to determine the control influence matrix, and 2) on the inversion of the state transition matrix (STM) associated with a set of linear equations of relative motion. In Ref. [1] the authors addressed the issues of establishing and reconfiguring a multi-spacecraft formation consisting of a central chief satellite surrounded by four deputy spacecraft using impulsive control under the assumption of two-body orbital mechanics. They proposed an analytical two-impulse control scheme for transferring a deputy spacecraft from a given location in the initial configuration to any given final configuration using the GVE and a linear relative dynamics model characterized in terms of nonsingular orbital element differences. Ichimura and Ichikawa developed an analytical open-time minimum fuel impulsive strategy associated with the Hill-Clohessy-Wiltshire equations of relative motion. The approach involves three in-plane impulses to achieve the optimal in-plane reconfiguration [2]. Chernick et al. addressed the computation of fuel-optimal control solutions for formation reconfiguration using impulsive maneuvers [3]. They developed semi-analytical solutions for in-plane and out-of-plane reconfigurations in near-circular J_2-perturbed and eccentric unperturbed orbits, using the relative orbit elements (ROE) to parameterize the equations of relative motion. More recently, Lawn et al. proposed a continuous low-thrust strategy based on the input-shaping technique for the short-distance planar spacecraft rephasing and rendezvous maneuvering problems [4]. The analytical solution was obtained by exploiting the Schweighart and Sedwick (SS) linear dynamics model.

Additionally, the growing use of small spacecraft for formation flying missions poses new challenges for reconfiguration maneuvering. Due to

* Corresponding author.
** Corresponding author.
E-mail addresses: gdimauro@ufl.edu (G. Di Mauro), bevilr@ufl.edu (R. Bevilacqua).

https://doi.org/10.1016/j.actaastro.2018.01.043
Received 3 August 2017; Received in revised form 14 January 2018; Accepted 23 January 2018
Available online 2 March 2018

the vehicles' limited size, small spacecraft are typically equipped with small thrusters which only operate in continuous mode to deliver low thrust. Many numerical methods have been investigated for the computation of the minimum-fuel reconfiguration maneuver using continuous low-thrust propulsion system. Steindorf et al. proposed a continuous control strategy for formations operating in perturbed orbits of arbitrary eccentricity [5]. They derived a control law based on the Lyapunov theory and ROE dynamics parameterization, and implemented guidance algorithms based on potential fields. This approach allowed time constraints, thrust level constraints, wall constraints, and passive collision avoidance constraints to be included in the guidance strategy. Richards et al. proposed fuel-optimal control algorithm by using the linear time-varying Hill–Clohessy–Wiltshire relative dynamics model. The trajectory optimization approach were based on the solution of a mixed-integer linear programming (MILP) problem [6]. Huntington et al. developed a nonlinear fuel-optimal configuration method for tetrahedral formation based on Gauss variational equations. The associated optimization problem is solved using Gauss pseudospectral method [7]. Massari et al. proposed a nonlinear low-thrust trajectory optimization method using a combination of parallel multiple shooting direct transcription and a barrier interior point method. They exploited a nonlinear dynamics model to describe the relative motion considering any kind of positional force field [8].

Ultimately, future formation flying missions will need to operate autonomously to enhance the mission performance, increase the mission robustness/flexibility, and reduce the overall costs. The achievement of such on-board autonomy requires the development of formation control algorithms that are able to efficiently provide a solution on-board without scarifying the maneuvering accuracy, [9].

In light of the above challenges, this work addresses the design of a computationally efficient strategy for the reconfiguration of a formation in J_2-perturbed near-circular orbits using a finite number of finite-time maneuvers. The main contributions of this work are:

- the development of a linearized relative dynamics model and the derivation of the corresponding closed-form solution. In further details, the results previously published in Ref. [10] are extended by computing the input matrix and the corresponding convolution matrix. In the framework of spacecraft relative motion, different dynamics models have been developed over the years, based on different state representation and subject to a multitude of constraints and limitations on the intersatellite range of applicability, the eccentricity of the satellite orbits, and the type of modeled perturbation forces, [11,12]. In this study the relative motion is parameterized in terms of relative orbit elements (ROE) taking into account the J_2 perturbation and the control accelerations.
- the derivation of the analytical and semi-analytical control solutions for the in-plane and out-of-plane formation reconfiguration problems, respectively, using a continuous acceleration profile.

The rest of the paper is organized as follows. In the first section, the differential equations (and their associated linearization) describing the relative motion of two Earth orbiting spacecraft under the effects of J_2 and continuous external accelerations are presented. A closed-form solution for the linearized relative motion is derived for near-circular orbit cases, i.e. for very small or zero eccentricity. The subsequent section is devoted to the derivation of control solutions for the in-plane, out-of-plane, and full spacecraft formation reconfiguration problems. Analytical and numerical approaches are proposed to efficiently compute a feasible reconfiguration maneuver. The final section shows the relative trajectories obtained using the developed control solutions, pointing out their performances in terms of maneuver cost and accuracy. In the same section a comparison with the minimum-fuel maneuver obtained using a global optimizer is also presented.

2. Relative dynamics model

In this section the dynamics model used to describe the relative motion between two spacecraft orbiting the Earth is presented. The model is formalized by using the ROE state as defined by D'Amico in Refs. [13,14], and allows for the inclusion of Earth oblateness J_2 and external constant acceleration effects.

2.1. Relative orbit elements

The absolute orbit of a satellite can be expressed by the set of classical Keplerian orbit elements, $\boldsymbol{\alpha} = [a, e, i, \omega, \Omega, M]^T$. The relative motion of a *deputy* spacecraft with respect to another one, referred to as *chief*, can be parameterized using the dimensionless relative orbit elements defined in Ref. [13] and here recalled for completeness,

$$\delta\boldsymbol{\alpha} = \begin{bmatrix} \dfrac{a_d}{a_c} - 1 \\ (M_d - M_c) + (\omega_d - \omega_c) + (\Omega_d - \Omega_c)\mathrm{c}_{i_c} \\ e_{x,d} - e_{x,c} \\ e_{y,d} - e_{y,c} \\ i_d - i_c \\ (\Omega_d - \Omega_c)\mathrm{s}_{i_c} \end{bmatrix} = \begin{bmatrix} \delta a \\ \delta\lambda \\ \delta e_x \\ \delta e_y \\ \delta i_x \\ \delta i_y \end{bmatrix} \tag{1}$$

In Eq. (1) the subscripts "c" and "d" label the chief and deputy satellites respectively, whereas $s_{(\bullet)} = \sin(\bullet)$ and $c_{(\bullet)} = \cos(\bullet)$. Moreover, $e_{x,(\bullet)} = e_{(\bullet)}\mathrm{c}_{\omega_{(\bullet)}}$ and $e_{y,(\bullet)} = e_{(\bullet)}\mathrm{s}_{\omega_{(\bullet)}}$ are defined as the components of the eccentricity vector and ω is the argument of perigee. The first two components of the relative state $\delta\boldsymbol{\alpha}$, are the relative semi-major axis, δa, and the relative mean longitude $\delta\lambda$, whereas the remaining components constitute the coordinates of the relative eccentricity vector, $\delta\boldsymbol{e}$, and relative inclination vector, $\delta\boldsymbol{i}$. It is worth remarking that the use of the ROE parameterization facilitates the inclusion of perturbing accelerations, such as Earth oblateness J_2 effects or atmospheric drag, into the dynamical model and offers an immediate insight into the relative motion geometry [14]. In addition, the above relative state is non-singular for circular orbits ($e_c = 0$), whereas it is still singular for strictly equatorial orbits ($i_c = 0$).

2.2. Non-linear equations of relative motion

The averaged variations of mean ROE (i.e. without short- and long-periodic terms) caused by the Earth's oblateness J_2 effects can be derived from the differentiation of chief and deputy mean classical elements, $\boldsymbol{\alpha}_c = [a_c, e_c, i_c, \omega_c, \Omega_c, M_c]^T$ and $\boldsymbol{\alpha}_d = [a_d, e_d, i_d, \omega_d, \Omega_d, M_d]^T$ respectively [15,16],

$$\dot{\boldsymbol{\alpha}}_{c,J2} = \begin{bmatrix} \dot{a}_c \\ \dot{e}_c \\ \dot{i}_c \\ \dot{\omega}_c \\ \dot{\Omega}_c \\ \dot{M}_c \end{bmatrix} = K_c \begin{bmatrix} 0_{3\mathbf{x}1} \\ Q_c \\ -2cos(i_c) \\ \eta_c P_c \end{bmatrix} \quad \dot{\boldsymbol{\alpha}}_{d,J2} = \begin{bmatrix} \dot{a}_d \\ \dot{e}_d \\ \dot{i}_d \\ \dot{\omega}_d \\ \dot{\Omega}_d \\ \dot{M}_d \end{bmatrix} = K_d \begin{bmatrix} 0_{3\mathbf{x}1} \\ Q_d \\ -2cos(i_d) \\ \eta_d P_d \end{bmatrix}, \tag{2}$$

where

$$K_j = \frac{\gamma n_j}{a_j^2 \eta_j^4} \qquad \eta_j = \sqrt{1 - e_j^2} \qquad n_j = \sqrt{\frac{\mu}{a_j^3}}$$
$$Q_j = 5\cos\left(i_j\right)^2 - 1 \quad P_j = 3\cos\left(i_j\right)^2 - 1 \quad \gamma = \frac{3}{4} J_2 R_E^2 \tag{3}$$

In Eq. (3) the subscript "j" stands for "c" and "d". J_2 indicates the second spherical harmonic of the Earth's geopotential, R_E the Earth's

equatorial radius and μ the Earth gravitational parameter. Computing the time derivative of mean ROE as defined in Eq. (1) and substituting Eq. (2) yields

$$\delta\dot{\boldsymbol{\alpha}}_{J2} = \begin{bmatrix} 0 \\ \left(\dot{M}_d - \dot{M}_c\right) + \left(\dot{\omega}_d - \dot{\omega}_c\right) + \left(\dot{\Omega}_d - \dot{\Omega}_c\right)c_{i_c} \\ -e_d s_{\omega_d}\dot{\omega}_d + e_c s_{\omega_c}\dot{\omega}_c \\ +e_d c_{\omega_d}\dot{\omega}_d - e_c c_{\omega_c}\dot{\omega}_c \\ 0 \\ \left(\dot{\Omega}_d - \dot{\Omega}_c\right)s_{i_c} \end{bmatrix} = \boldsymbol{\sigma}_{J2}(\boldsymbol{\alpha}_c, \boldsymbol{\alpha}_d) \tag{4}$$

with

$$\boldsymbol{\sigma}_{J2}(\boldsymbol{\alpha}_c, \boldsymbol{\alpha}_d) = \begin{bmatrix} 0 \\ (\eta_d P_d K_d - \eta_c P_c K_c) + (K_d Q_d - K_c Q_c) - 2(K_d \mathrm{c}_{i_d} - K_c \mathrm{c}_{i_c})\mathrm{c}_{i_c} \\ -e_{y,d} K_d Q_d + e_{y,c} K_c Q_c \\ e_{x,d} K_d Q_d - e_{x,c} K_c Q_c \\ 0 \\ -2(K_d \mathrm{c}_{i_d} - K_c \mathrm{c}_{i_c})\mathrm{s}_{i_c} \end{bmatrix} \tag{5}$$

In this study only the deputy is assumed to be maneuverable and capable of providing continuous thrust along x, y, and z directions of its own Radial-Tangential-Normal (RTN) reference frame (also known as Local Vertical Local Horizontal (LVLH)). The RTN frame consists of orthogonal basis vectors with x pointing along the deputy absolute radius vector, z pointing along the angular momentum vector of the deputy absolute orbit, and $y = z \times x$ completing the triad and pointing in the along-track direction. The change of mean ROE caused by a continuous control acceleration vector $\boldsymbol{f}$ can be determined through the well-known Gauss variational equations (GVE) [17,18]. In fact, as widely discussed in Ref. [18], the mean orbit elements can be reasonably approximated by the corresponding osculating elements since the Jacobian of the osculating-to-mean transformation is approximately a 6x6 identity matrix, with the off-diagonal terms being of order J_2 or smaller. In other words, the variations of osculating elements are directly reflected in corresponding mean orbit elements changes. In light of the above, the variation of mean ROE induced by the external force is

$$\delta\dot{\boldsymbol{\alpha}}_F = \begin{bmatrix} \frac{\dot{a}_d}{a_c} \\ \dot{M}_d + \dot{\omega}_d + \dot{\Omega}_d c_{i_c} \\ \dot{e}_d c_{\omega_d} - e_d s_{\omega_d}\dot{\omega}_d \\ \dot{e}_d s_{\omega_d} + e_d c_{\omega_d}\dot{\omega}_d \\ \dot{i}_d \\ \dot{\Omega}_d s_{i_c} \end{bmatrix} = \boldsymbol{\sigma}_{\boldsymbol{F}}(\boldsymbol{\alpha}_d, \boldsymbol{f}) = \boldsymbol{\Gamma}_{\boldsymbol{F}}(\boldsymbol{\alpha}_d)\boldsymbol{f}, \tag{6}$$

where the control acceleration vector $\boldsymbol{f}$ is expressed in the deputy RTN frame components as $\boldsymbol{f} = [f_x, f_y, f_z]^T$. The individual terms of the control influence matrix $\boldsymbol{\Gamma}_{\boldsymbol{F}}$ are reported in Appendix A.

The relative motion between the deputy and chief satellites is given by adding the contributions from Keplerian gravity, the J_2 perturbation, and the external force vector $\boldsymbol{f}$. The final set of nonlinear differential equations is

$$\delta\dot{\boldsymbol{\alpha}} = \begin{bmatrix} 0 \\ n_d - n_c \\ 0 \\ 0 \\ 0 \\ 0 \end{bmatrix} + \boldsymbol{\sigma}_{J2}(\boldsymbol{\alpha}_c, \boldsymbol{\alpha}_d) + \boldsymbol{\sigma}_{\boldsymbol{F}}(\boldsymbol{\alpha}_d, \boldsymbol{f}) = \boldsymbol{\xi}(\boldsymbol{\alpha}_c, \boldsymbol{\alpha}_d(\boldsymbol{\alpha}_c, \delta\boldsymbol{\alpha}), \boldsymbol{f}). \tag{7}$$

Note that the function $\boldsymbol{\xi}(\boldsymbol{\alpha}_c, \boldsymbol{\alpha}_d(\boldsymbol{\alpha}_c, \delta\boldsymbol{\alpha}), \boldsymbol{f})$ can be reformulated in terms of $\boldsymbol{\alpha}_c$ and $\delta\boldsymbol{\alpha}$ using the following identities [16],

$$\begin{aligned} a_d &= a_c\delta a + a_c, \quad e_d = \sqrt{\left(e_c c_{\omega_c} + \delta e_x\right)^2 + \left(e_c s_{\omega_c} + \delta e_y\right)^2} \\ i_d &= i_c + \delta i_x, \quad M_d = M_c + \delta\lambda - (\omega_d - \omega_c) - (\Omega_d - \Omega_c)\mathrm{c}_{i_c}\delta i_x \\ \omega_d &= \tan^{-1}\left(\frac{e_c s_{\omega_c} + \delta e_y}{e_c c_{\omega_c} + \delta e_x}\right), \quad \Omega_d = \Omega_c + \frac{\delta i_y}{s_{i_c}} \end{aligned} \tag{8}$$

such that $\delta\dot{\boldsymbol{\alpha}} = \boldsymbol{\xi}(\boldsymbol{\alpha}_c, \delta\boldsymbol{\alpha}, \boldsymbol{f})$.

2.3. Linearized equations of relative motion

In order to obtain the linearized equations of relative motion, $\delta\dot{\boldsymbol{\alpha}}$ in Eq. (7) can be expanded about the chief orbit (i.e., $\delta\boldsymbol{\alpha} = 0$ and $\boldsymbol{f} = 0$) to first order using a Taylor expansion,

$$\delta\dot{\boldsymbol{\alpha}}(t) = \left[\frac{\partial\boldsymbol{\xi}}{\partial\delta\boldsymbol{\alpha}}\right]_{\substack{\delta\alpha = 0 \\ f = 0}} \delta\boldsymbol{\alpha}(t) + \left[\frac{\partial\boldsymbol{\xi}}{\partial\boldsymbol{f}}\right]_{\substack{\delta\alpha = 0 \\ f = 0}} \boldsymbol{f} = \boldsymbol{A}(\boldsymbol{\alpha}_c(t))\,\delta\boldsymbol{\alpha}(t) + \boldsymbol{B}(\boldsymbol{\alpha}_c(t))\boldsymbol{f}. \tag{9}$$

The matrices $\boldsymbol{A}$ and $\boldsymbol{B}$ represent the plant and input matrices, respectively. Under the assumption of near-circular chief orbit (i.e., $e_c \to 0$), these matrices are given by

$$\boldsymbol{A}_{NC} = \begin{bmatrix} 0 & 0 & 0 & 0 & 0 & 0 \\ -\Lambda_c & 0 & 0 & 0 & -K_c F_c S_c & 0 \\ 0 & 0 & 0 & -K_c Q_c & 0 & 0 \\ 0 & 0 & K_c Q_c & 0 & 0 & 0 \\ 0 & 0 & 0 & 0 & 0 & 0 \\ \frac{7K_c S_c}{2} & 0 & 0 & 0 & 2K_c T_c & 0 \end{bmatrix}, \tag{10}$$

$$\boldsymbol{B}_{NC} = \frac{1}{n_c a_c}\begin{bmatrix} 0 & 2 & 0 \\ -2 & 0 & 0 \\ s_{u_c} & 2c_{u_c} & 0 \\ -c_{u_c} & 2s_{u_c} & 0 \\ 0 & 0 & c_{u_c} \\ 0 & 0 & s_{u_c} \end{bmatrix}, \tag{11}$$

where $u_c = \omega_c + M_c$ denotes the mean argument of latitude of chief orbit and the following substitutions are applied for clarity

$$\begin{aligned} F_c &= 4 + 3\eta_c, \quad E_c = 1 + \eta_c, \quad S_c = \sin(2i_c), \\ T_c &= \sin(i_c)^2, \quad \Lambda_c = \frac{3}{2}n_c + \frac{7}{2}E_c K_c P_c. \end{aligned} \tag{12}$$

For an analysis of the applicability range of the linear relative dynamics model (9)–(11) we address the reader to [14].

2.4. Analytical solution for near-circular linear dynamics model

The solution of the linear system (9), $\delta\boldsymbol{\alpha}(t)$, can be expressed as a function of the initial ROE state vector $\delta\boldsymbol{\alpha}(t_0)$, and the constant forcing vector, $\boldsymbol{f}$, i.e. as

$$\delta\boldsymbol{\alpha}(t) = \boldsymbol{\Phi}(t, t_0)\delta\boldsymbol{\alpha}(t_0) + \boldsymbol{\Psi}(t, t_0)\boldsymbol{f} \tag{13}$$

where $\boldsymbol{\Phi}(t, t_0)$ and $\boldsymbol{\Psi}(t, t_0)$ indicate the STM and the convolution matrix, respectively. As widely discussed in Refs. [10,16], Floquet theory can be exploited to derive the STM. The STM associated with near-circular linear relative dynamics model is reported here for completeness

$$\boldsymbol{\Phi}_{NC}(t,t_0)=\begin{bmatrix}1&0&0&0&0&0\\-\Lambda_c\Delta t&1&0&0&-K_cF_cS_c\Delta t&0\\0&0&c_{\Delta\omega}&-s_{\Delta\omega}&0&0\\0&0&s_{\Delta\omega}&c_{\Delta\omega}&0&0\\0&0&0&0&1&0\\\frac{7}{2}K_cS_c\Delta t&0&0&0&2K_cT_c\Delta t&1\end{bmatrix} \tag{14}$$

where $\Delta t = t - t_0$ and $\Delta\omega = K_cQ_c\Delta t$. According to linear dynamics system theory [19], the convolution matrix, $\boldsymbol{\Psi}(t,t_0)$, can be computed by solving the following integral,

$$\boldsymbol{\Psi}_{NC}(t,t_0)=\int_{t_0}^{t}\boldsymbol{\Phi}_{NC}(t,\tau)\boldsymbol{B}_{NC}(\boldsymbol{\alpha}_c(\tau))d\tau \tag{15}$$

Note that the integrand of the integral (15) does not include the control vector since $\boldsymbol{f}$ is assumed to be constant over the interval $[t_0,t]$. Substituting the STM and the $\boldsymbol{B}_{NC}$ matrices reported in Eqs. (14) and (10), respectively, into Eq. (15) yields

$$\boldsymbol{\Psi}_{NC}(t\ ,t_0)=\begin{bmatrix}0&\frac{2\Delta u}{n_ca_cW_c}&0\\-\frac{2\Delta u}{n_ca_cW_c}&-\frac{\Lambda_c\Delta u^2}{n_ca_cW_c^2}&\psi_{23}\\-\frac{c_{u_{c,t}}-c_{u_{c,0}+C\Delta u}}{n_ca_c(1-C)W_c}&2\frac{s_{u_{c,t}}-s_{u_{c,0}+C\Delta u}}{n_ca_c(1-C)W_c}&0\\-\frac{s_{u_{c,t}}-s_{u_{c,0}+C\Delta u}}{n_ca_c(1-C)W_c}&-2\frac{c_{u_{c,t}}-c_{u_{c,0}+C\Delta u}}{n_ca_c(1-C)W_c}&0\\0&0&\frac{s_{u_{c,t}}-s_{u_{c,0}}}{n_ca_cW_c}\\0&\frac{7}{2}\frac{K_cS_c\Delta u^2}{n_ca_cW_c^2}&\psi_{63}\end{bmatrix} \tag{16}$$

$$\psi_{23}=\frac{F_cK_cS_c\left(c_{u_{c,t}}-c_{u_{c,0}}+s_{u_{c,0}}\Delta u\right)}{n_ca_cW_c^2}\qquad \psi_{63}=\left(-\frac{(W_c+2K_cT_c)\left(c_{u_{c,t}}-c_{u_{c,0}}\right)}{n_ca_cW_c^2}-\frac{2K_cT_cs_{u_{c,0}}\Delta u}{n_ca_cW_c^2}\right)$$

where $u_{c,t}$ and $u_{c,0}$ are the mean argument of latitude of chief orbit at the instant t and t_0, respectively, and $\Delta u = u_{c,t} - u_{c,0}$. In Eq. (16) the terms C and W_c are constant coefficients that depend on the mean semi-major axis, eccentricity, and inclination of the chief orbit as follows

$$W_c = n_c + K_cQ_c + \eta_cK_cP_c,\quad C=\frac{K_cQ_c}{W_c}. \tag{17}$$

Note that the mean argument of the latitude can be written as a function of time using the relationships reported in Eq. (2), i.e., $u_{c,t} = u_{c,0} + W_c(t - t_0)$.

3. Reconfiguration control problem

This section presents the derivation of a control solution for the reconfiguration problem, using a finite number of finite-time maneuvers. Recall that the trajectory reconfiguration problem denotes the achievement of a certain user-defined set of ROE after a given time interval. Again, only the deputy is assumed to be maneuverable and capable of providing a piecewise continuous thrust along the x, y, and z directions of its own RTN reference frame.

3.1. General approach

Let us consider N_x continuous maneuvers along x direction of magnitude $f_{x,j}$ and duration $\Delta t_{j,x} = t_{j,x,f} - t_{j,x,0}$, with $j = 1, \ldots N_x$, as illustrated in Fig. 1. Using the near-circular linearized model discussed in section 2.3, the relative state at the end of each j-th maneuvers $\delta\boldsymbol{\alpha}(t_{j,x,f})$ can be expressed as a function of $\delta\boldsymbol{\alpha}(t_{j,x,0})$, the maneuver duration $\Delta t_{j,x}$, and maneuver magnitude, $f_{x,j}$, as follows (see Eq. (13)),

$$\delta\boldsymbol{\alpha}_{j,f}=\delta\boldsymbol{\alpha}\left(t_{j,x,f}\right)=\boldsymbol{\Phi}\left(t_{j,x,f},t_{j,x,0}\right)\delta\boldsymbol{\alpha}\left(t_{j,x,0}\right)+\boldsymbol{\Psi}\left(t_{j,x,f},t_{j,x,0}\right)\begin{bmatrix}f_{x,j}\\0\\0\end{bmatrix}. \tag{18}$$

$t_{j,x,0}$ and $t_{j,x,f}$ indicate the initial and the final times of the j-th maneuver along x direction respectively. Note that the instant time $t_{j,x,f}$ can be expressed as a function of the maneuver duration $\Delta t_{j,x}$ as $t_{j,x,f} = t_{j,x,0} + \Delta t_{j,x}$. According to Eq. (18), the mean ROE at the end of the maneuvering interval, $\delta\boldsymbol{\alpha}(t_m)$, depend on the mean ROE at the initial maneuver time $\delta\boldsymbol{\alpha}(t_0)$, on the N_x maneuvers' durations, $\Delta t_{j,x}$, and on the maneuvers' magnitudes, $f_{x,j}$,

$$\delta\boldsymbol{\alpha}_{1,0}=\delta\boldsymbol{\alpha}(t_{1,x,0})=\boldsymbol{\Phi}(t_{1,x,0},t_0)\delta\boldsymbol{\alpha}(t_0)=\boldsymbol{\Phi}(t_{1,x,0},t_0)\delta\boldsymbol{\alpha}_0 \tag{19}$$

$$\delta\boldsymbol{\alpha}_{1,f}=\boldsymbol{\Phi}\left(t_{1,x,f},t_0\right)\delta\boldsymbol{\alpha}_0+\boldsymbol{\Psi}\left(t_{1,x,f},t_{1,x,0}\right)\begin{bmatrix}f_{x,1}\\0\\0\end{bmatrix} \tag{20}$$

$$\begin{aligned}\delta\boldsymbol{\alpha}_{2,0}&=\boldsymbol{\Phi}\left(t_{2,x,0},t_{1,x,f}\right)\delta\boldsymbol{\alpha}_{1,f}\\&=\boldsymbol{\Phi}(t_{2,x,0},t_0)\delta\boldsymbol{\alpha}_0+\boldsymbol{\Phi}\left(t_{2,x,0},t_{1,x,f}\right)\boldsymbol{\Psi}\left(t_{1,x,f},t_{1,x,0}\right)\begin{bmatrix}f_{x,1}\\0\\0\end{bmatrix}\end{aligned} \tag{21}$$

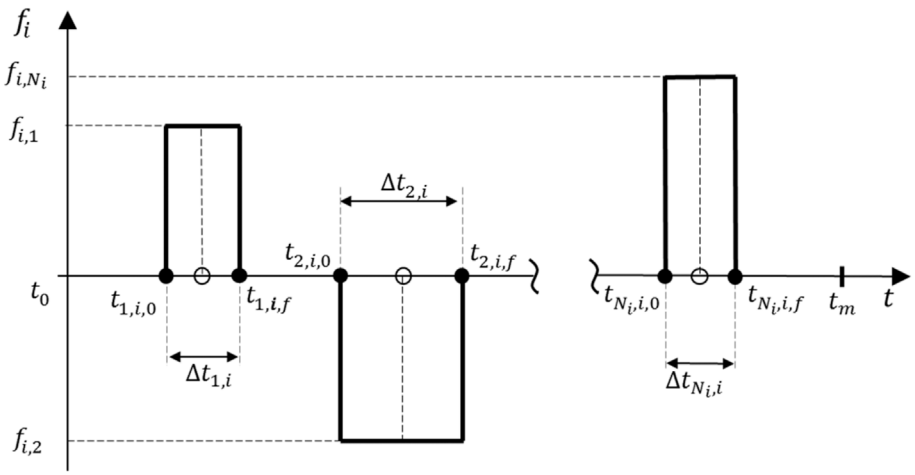

Fig. 1. Continuous control profile ($\boldsymbol{i} = \boldsymbol{x},\boldsymbol{y},\boldsymbol{z}$).

$$\delta\boldsymbol{\alpha}_{2,f} = \boldsymbol{\Phi}\left(t_{2,x,f}, t_{2,x,0}\right)\delta\boldsymbol{\alpha}_{2,0} + \boldsymbol{\Psi}\left(t_{2,x,f}, t_{2,x,0}\right)\begin{bmatrix} f_{x,2} \\ 0 \\ 0 \end{bmatrix}$$
$$= \boldsymbol{\Phi}(t_{2,x,0}, t_0)\delta\boldsymbol{\alpha}_0 + \boldsymbol{\Phi}\left(t_{2,x,f}, t_{1,x,f}\right)\boldsymbol{\Psi}\left(t_{1,x,f}, t_{1,x,0}\right)\begin{bmatrix} f_{x,1} \\ 0 \\ 0 \end{bmatrix} + \boldsymbol{\Psi}\left(t_{2,x,f}, t_{2,x,0}\right) \times \begin{bmatrix} f_{x,2} \\ 0 \\ 0 \end{bmatrix} \tag{22}$$

$$\delta\boldsymbol{\alpha}_{t_m} = \boldsymbol{\Phi}(t_m, t_0)\delta\boldsymbol{\alpha}_0 + \sum_{j=1}^{N_x}\boldsymbol{\Phi}\left(t_m, t_{j,x,f}\right)\boldsymbol{\Psi}\left(t_{j,x,f}, t_{j,x,0}\right)\begin{bmatrix} f_{x,j} \\ 0 \\ 0 \end{bmatrix}. \tag{23}$$

When the control thrust has a component along each RTN reference frame axis, the change of mean ROE vector at the end of the maneuvering interval is given by,

$$\delta\boldsymbol{\alpha}_{t_m} = \boldsymbol{\Phi}(t_m, t_0)\delta\boldsymbol{\alpha}_0 + \boldsymbol{\varsigma}_x + \boldsymbol{\varsigma}_y + \boldsymbol{\varsigma}_z \tag{24}$$

where

$$\begin{aligned}
\boldsymbol{\varsigma}_x &= \sum_{j=1}^{N_x}\boldsymbol{\Phi}\left(t_m, t_{j,x,f}\right)\boldsymbol{\Psi}\left(t_{j,x,f}, t_{j,x,0}\right)\begin{bmatrix} f_{x,j} \\ 0 \\ 0 \end{bmatrix} \\
\boldsymbol{\varsigma}_y &= \sum_{j=1}^{N_y}\boldsymbol{\Phi}\left(t_m, t_{j,y,f}\right)\boldsymbol{\Psi}\left(t_{j,y,f}, t_{j,y,0}\right)\begin{bmatrix} 0 \\ f_{y,j} \\ 0 \end{bmatrix} \\
\boldsymbol{\varsigma}_z &= \sum_{j=1}^{N_z} + \boldsymbol{\Phi}\left(t_m, t_{j,z,f}\right)\boldsymbol{\Psi}\left(t_{j,z,f}, t_{j,z,0}\right)\begin{bmatrix} 0 \\ 0 \\ f_{z,j} \end{bmatrix}.
\end{aligned} \tag{25}$$

with $\boldsymbol{\varsigma}_i = \begin{bmatrix} \boldsymbol{\varsigma}_i^{ip} \\ \boldsymbol{\varsigma}_i^{oop} \end{bmatrix} \in \mathbb{R}^6$, $\boldsymbol{\varsigma}_i^{ip} \in \mathbb{R}^4$, $\boldsymbol{\varsigma}_i^{oop} \in \mathbb{R}^2$, and $i = x, y, z$. The reconfiguration problem is described by the following expression

$$\Delta\delta\boldsymbol{\alpha}_{des} = \delta\boldsymbol{\alpha}_{des} - \boldsymbol{\Phi}(t_m, t_0)\delta\boldsymbol{\alpha}_0 = \boldsymbol{\varsigma}_x + \boldsymbol{\varsigma}_y + \boldsymbol{\varsigma}_z, \tag{26}$$

where the term $\delta\boldsymbol{\alpha}_{des}$ is the desired mean ROE vector at the end of the maneuvering interval. Eq. (26) represents a set of 6 nonlinear equations in $3N_x + 3N_y + 3N_z$ unknowns, i.e. the maneuvers' magnitudes $f_{i,j}$, their application times, $t_{j,i,0}$ (or alternatively the time of the middle point of the maneuver, i.e. $(t_{j,i,0} + t_{j,i,f})/2$), and the maneuvers' durations, $\Delta t_{j,i}$, with $i = , x, y, z$. Note that the maneuvers-locations and durations will be expressed in terms of mean argument of latitude throughout the paper, since the linear relationship that exists between the time and mean argument of latitude, i.e. $u_{c,t} = u_{c,0} + W_c(t - t_0)$. The vector $\delta\boldsymbol{\alpha}_0$ is assumed to be known. According to Eq. (26), at least two maneuvers are needed to obtain a finite number of analytical solutions.

In Ref. [3] the authors derived the semi-analytical solutions for the in-plane and out-of-plane reconfiguration problems in near-circular perturbed orbits using an impulsive maneuver scheme. This paper presents the analytical and semi-analytical solutions for the same class of problems using continuous thrust maneuvers, and addresses the problem of full spacecraft formation reconfiguration. More specifically, the following reconfiguration problems are considered:

- *In-plane reconfiguration*:

$$S_1 = \left\{\Delta\delta\widehat{\boldsymbol{\alpha}}_{des}^{ip} = \left[\Delta\delta a_{des}, \Delta\delta\lambda_{des}, \Delta\delta e_{x,des}, \Delta\delta e_{y,des}\right]^T \subseteq \Delta\delta\boldsymbol{\alpha}_{des}\right\};$$

- *Out-of-plane reconfiguration*:

$$S_2 = \left\{\Delta\delta\widehat{\boldsymbol{\alpha}}_{des}^{oop} = \left[\Delta\delta i_{x,des}, \Delta\delta i_{y,des}\right]^T \subseteq \Delta\delta\boldsymbol{\alpha}_{des}\right\};$$

- *Full reconfiguration:*

$$S_3 = \left\{\Delta\delta\widehat{\boldsymbol{\alpha}}_{des}^{full} = \left[\Delta\delta a_{des}, \Delta\delta\lambda_{des}, \Delta\delta\boldsymbol{e}_{des}, \Delta\delta\boldsymbol{i}_{des}\right]^T\right\}$$

The control solutions are obtained using the STM and convolution matrices associated with the near-circular dynamics model (see Eq. (14) and Eq. (16)).

3.2. In-plane reconfiguration

In this section the in-plane reconfiguration problem is addressed. Let us consider that only three tangential maneuvers are performed by the deputy spacecraft $f_{y,1}$, $f_{y,2}$, and $f_{y,3}$. This choice allows an analytical solution to be computed. Moreover, as discussed by Chernick et al. in Ref. [3], the use of three tangential impulses allows finding a minimum delta-V solution when the reconfiguration cost is driven by the variation of relative eccentricity vector. For this reason, the approach in this paper focuses on a similar tangential maneuvering scheme.

According to Eq. (24), the equations governing the evolution of the in-plane mean ROE are

$$\tilde{u}_{1,y}f_{y,1} + \tilde{u}_{2,y}f_{y,2} + \tilde{u}_{3,y}f_{y,3} = \frac{W_c n_c a_c}{4}\Delta\delta a_{des} \tag{27}$$

$$\begin{aligned}
&-\left(2\Lambda_c\left(u_{t_m} - \widehat{u}_{1,y}\right)\tilde{u}_{1,y}\right)f_{y,1} - \left(2\Lambda_c\left(u_{t_m} - \widehat{u}_{2,y}\right)\tilde{u}_{2,y}\right)f_{y,2} - \left(2\Lambda_c\left(u_{t_m}\right.\right. \\
&\left.\left. - \widehat{u}_{3,y}\right)\tilde{u}_{3,y}\right)f_{y,3} \\
&= \frac{W_c^2 n_c a_c}{2}\Delta\delta\lambda_{des}
\end{aligned} \tag{28}$$

$$\begin{aligned}
&\left(\cos\left(Cu_{t_m} + (1-C)\widehat{u}_{1,y}\right)\sin\left((1-C)\tilde{u}_{1,y}\right)\right)f_{y,1} + \left(\cos\left(Cu_{t_m}\right.\right. \\
&\left.\left. + (1-C)\widehat{u}_{2,y}\right)\sin\left((1-C)\tilde{u}_{2,y}\right)\right)f_{y,2} + \left(\cos\left(Cu_{t_m} + (1-C)\widehat{u}_{3,y}\right)\sin\right. \\
&\left.\left(\times(1-C)\tilde{u}_{3,y}\right)\right)f_{y,3} \\
&= \frac{(1-C)W_c n_c a_c}{4}\Delta\delta e_{x,des}
\end{aligned} \tag{29}$$

$$\begin{aligned}
&\left(\sin\left(Cu_{t_m} + (1-C)\widehat{u}_{1,y}\right)\sin\left((1-C)\tilde{u}_{1,y}\right)\right)f_{y,1} + \left(\sin\left(Cu_{t_m}\right.\right. \\
&\left.\left. + (1-C)\widehat{u}_{2,y}\right)\sin\left((1-C)\tilde{u}_{2,y}\right)\right)f_{y,2} + \left(\sin\left(Cu_{t_m} + (1-C)\widehat{u}_{3,y}\right)\sin\right. \\
&\left.\left(\times(1-C)\tilde{u}_{3,y}\right)\right)f_{y,3} \\
&= \frac{(1-C)W_c n_c a_c}{4}\Delta\delta e_{y,des}
\end{aligned} \tag{30}$$

where

$$\widehat{u}_{j,y} = \frac{u_{j,f} + u_{j,0}}{2} \quad \tilde{u}_{j,y} = \frac{u_{j,f} - u_{j,0}}{2} \quad j = 1, \ldots 3 \tag{31}$$

and $u_{j,0}$ and $u_{j,f}$ denote the chief mean argument of latitude at times $t_{j,y,0}$ and $t_{j,y,f}$, respectively. Defining the variables

$$\overline{U}_{j,0,y} = (1-C)u_{j,0,y} + Cu_{t_m}, \quad \overline{U}_{j,f,y} = (1-C)u_{j,f,y} + Cu_{t_m} \tag{32}$$

$$\begin{aligned}
\widetilde{\overline{U}}_{j,y} &= \frac{\overline{U}_{j,f,y} - \overline{U}_{j,0,y}}{2} = (1-C)\tilde{u}_{j,y} \quad j = 1, .., 3 \\
\widehat{\overline{U}}_{j,y} &= \frac{\overline{U}_{j,f,y} + \overline{U}_{j,0,y}}{2} = Cu_{t_m} + (1-C)\widehat{u}_{j,y}
\end{aligned} \tag{33}$$

allows for rearranging Eqs. (27)–(31) into a more convenient form, given by

$$\widehat{\overline{U}}_{1,y}f_{y,1} + \widetilde{\overline{U}}_{2,y}f_{y,2} + \widetilde{\overline{U}}_{3,y}f_{y,3} = \frac{(1-C)W_c n_c a_c}{4}\Delta\delta a_{des} \tag{34}$$

$$-\left(2\Lambda_c\left(u_{t_m}-\widehat{\overline{U}}_{1,y}\right)\widetilde{\overline{U}}_{1,y}\right)f_{y,1}-\left(2\Lambda_c\left(u_{t_m}-\widehat{\overline{U}}_{2,y}\right)\widetilde{\overline{U}}_{2,y}\right)f_{y,2}$$
$$-\left(2\Lambda_c\left(u_{t_m}-\widehat{\overline{U}}_{3,y}\right)\widetilde{\overline{U}}_{3,y}\right)f_{y,3}=\frac{(1-C)^2W_c^2n_ca_c}{2}\Delta\delta\lambda_{des} \tag{35}$$

$$\left(\cos\left(\widehat{\overline{U}}_{1,y}\right)\sin\left(\widetilde{\overline{U}}_{1,y}\right)\right)f_{y,1}+\left(\cos\left(\widehat{\overline{U}}_{2,y}\right)\sin\left(\widetilde{\overline{U}}_{2,y}\right)\right)f_{y,2}$$
$$+\left(\cos\left(\widehat{\overline{U}}_{3,y}\right)\sin\left(\widetilde{\overline{U}}_{3,y}\right)\right)f_{y,3}=\frac{(1-C)W_cn_ca_c}{4}\Delta\delta e_{x,des} \tag{36}$$

$$\left(\sin\left(\widehat{\overline{U}}_{1,y}\right)\sin\left(\widetilde{\overline{U}}_{1,y}\right)\right)f_{y,1}+\left(\sin\left(\widehat{\overline{U}}_{2,y}\right)\sin\left(\widetilde{\overline{U}}_{2,y}\right)\right)f_{y,2}$$
$$+\left(\sin\left(\widehat{\overline{U}}_{3,y}\right)\sin\left(\widetilde{\overline{U}}_{3,y}\right)\right)f_{y,3}=\frac{(1-C)W_cn_ca_c}{4}\Delta\delta e_{y,des} \tag{37}$$

It is worth noting that Eqs. (34)–(37) match the expressions obtained for three tangential impulses maneuver in Ref. [3]. Accordingly, the solution of the above system will have the same structure. In light of this, the locations (expressed as mean argument of latitude) of the maneuver middle points, $\widehat{u}_{j,y}$, are given by

$$\widehat{u}_{j,y}=\frac{\widehat{\overline{U}}_{j,y}}{1-C}-\frac{Cu_{t_m}}{1-C}\quad j=1,\ldots,3$$
$$\overline{U}=\operatorname{atan}\left(\frac{\Delta\delta e_{y,des}}{\Delta\delta e_{x,des}}\right) \tag{38}$$
$$\widehat{\overline{U}}_{1,y}=\overline{U}+k_1\pi\quad\widehat{\overline{U}}_{2,y}=\widehat{\overline{U}}_{1,y}+k_2\pi\quad\widehat{\overline{U}}_{3,y}=\widehat{\overline{U}}_{1,y}+k_3\pi$$

where k_j must be an integer number. The thrust magnitudes are

$$f_{y,j}=-\frac{\left\{(-1)^{k_1}(1-C)W_ca_cn_c\Xi_j\right\}}{D}. \tag{39}$$

where the quantities Ξ_j and D are detailed in Appendix B. It is worth remarking that the solution (38)–(39) is determined by assuming that the maneuvers' locations, $\tilde{u}_{j,y}$ (or $\widetilde{\overline{U}}_{j,y}$) with $j=1,\ldots,3$, are user-defined parameters, i.e. by reducing the number of unknowns from 9 to 6. Otherwise, a numerical approach should be used to solve nonlinear system (38)–(39).

3.3. Out-of-plane reconfiguration

In this section the out-of-plane control solution is presented. In order to achieve the desired x and y components of the relative inclination vector at the end of the maneuver, the control solution must include a component in the cross-track (z) direction. In fact, the only way to modify the difference in chief and deputy orbit inclination (i.e., δi_x) is to provide a control acceleration along the z-axis of deputy RTN frame. This is immediately evident from inspection of the linearized equations of relative motion (see Eq. (10)). If only a single cross-track maneuver is performed by the deputy satellite, the equations governing the change of relative inclination vector are (see Eq. (24))

$$\cos(\widehat{u}_{1,z})\sin(\tilde{u}_{1,z})f_{z,1}=\frac{W_cn_ca_c}{2}\Delta\delta i_{x,des} \tag{40}$$

$$\begin{pmatrix}2K_cT_c(u_{t_m}-\widehat{u}_{1,z}-\tilde{u}_{1,z})\cos(\widehat{u}_{1,z})\sin(\tilde{u}_{1,z})+\\(W_c+2K_cT_c)\sin(\widehat{u}_{1,z})\sin(\tilde{u}_{1,z})\\-2K_cT_c\sin(\widehat{u}_{1,z}-\tilde{u}_{1,z})\tilde{u}_{1,z}\end{pmatrix}f_{z,1}=\frac{W_c^2n_ca_c}{2}\Delta\delta i_{y,des}. \tag{41}$$

The magnitude of the maneuver can be computed by inverting Eq. (40),

$$f_{z,1}=\frac{W_cn_ca_c}{2[\cos(\widehat{u}_{1,z})\sin(\tilde{u}_{1,z})]}\Delta\delta i_{x,des}. \tag{42}$$

If the maneuver duration, $\tilde{u}_{1,z}$, is a user-defined parameter, the location of the maneuver, $\widehat{u}_{1,z}$, can be found by substituting Eq. (42) into Eq. (41) to obtain the following transcendental expression,

$$2K_cT_c(u_{t_m}-\widehat{u}_{1,z}-\tilde{u}_{1,z})+(W_c+2K_cT_c)\operatorname{tg}(\widehat{u}_{1,z})-\frac{2K_cT_c\sin(\widehat{u}_{1,z}-\tilde{u}_{1,z})\tilde{u}_{1,z}}{\cos(\widehat{u}_{1,z})\sin(\tilde{u}_{1,z})}$$
$$=W_c\frac{\Delta\delta i_{y,des}}{\Delta\delta i_{x,des}}. \tag{43}$$

Eq. (43) can be numerically solved by using an iterative algorithm such as the bisection or Newton-Raphson methods [20]. In this study the Brent's method [20] implemented in *fzero* Matlab routine is used for the solution of Eq. (43). The single out-of-plane maneuver solution for unperturbed orbits provides useful insight into choosing a good initial guess for quick convergence of the iterative approach. Alternatively, a parametric analysis of the error function,

$$J=2K_cT_c(u_{t_m}-\widehat{u}_{1,z}-\tilde{u}_{1,z})+(W_c+2K_cT_c)\operatorname{tg}(\widehat{u}_{1,z})$$
$$-\frac{2K_cT_c\sin(\widehat{u}_{1,z}-\tilde{u}_{1,z})\tilde{u}_{1,z}}{\cos(\widehat{u}_{1,z})\sin(\tilde{u}_{1,z})}-W_c\frac{\Delta\delta i_{y,des}}{\Delta\delta i_{x,des}}, \tag{44}$$

is needed to determine the initial guess for the iterative algorithm.

It is worth pointing out that, under the assumptions of using a single finite-time maneuver with a given duration, the out-of-plane reconfiguration problem is reduced to the solution of a nonlinear equation (see Eq. (43)) for the determination of the maneuver location. In fact, the maneuver magnitude is analytically computed through the expression (42). It must be remarked, however, that the proposed approach only guarantees the achievement of the final desired relative configuration.

3.4. Full reconfiguration

In this section the solution of the full reconfiguration problem is presented. Without loss of generality, the full reconfiguration is achieved through three tangential finite-time maneuvers and one single out-of-plane maneuver. At least one cross-track maneuver is needed to change the relative inclination vector. Moreover, no radial maneuvers are considered since they are more demanding in terms of delta-V than tangential ones for the in-plane motion control, [13]. Assuming that the maneuvers' durations are user-defined parameters, the following set of six equations must be solved with respect to the unknowns magnitudes and locations, $f_{y,j}$, $f_{z,1}$, $\widehat{u}_{j,y}$ and $\widehat{u}_{1,z}$ ($j=1,\ldots3$), respectively

$$\tilde{u}_{1,y}f_{y,1}+\tilde{u}_{2,y}f_{y,2}+\tilde{u}_{3,y}f_{y,3}=\frac{W_cn_ca_c}{4}\Delta\delta a_{des} \tag{45}$$

$$-\left(2\Lambda_c\left(u_{t_m}-\widehat{u}_{1,y}\right)\tilde{u}_{1,y}\right)f_{y,1}-\left(2\Lambda_c\left(u_{t_m}-\widehat{u}_{2,y}\right)\tilde{u}_{2,y}\right)f_{y,2}-\left(2\Lambda_c\left(u_{t_m}\right.\right.$$
$$\left.\left.-\widehat{u}_{3,y}\right)\tilde{u}_{3,y}\right)f_{y,3}+F_cK_cS_c\begin{pmatrix}-\sin(\widehat{u}_{1,z})\sin(\tilde{u}_{1,z})+\sin(\widehat{u}_{1,z}-\tilde{u}_{1,z})\tilde{u}_{1,z}+\ldots\\\ldots-(u_{t_m}-\widehat{u}_{1,z}-\tilde{u}_{1,z})\cos(\widehat{u}_{1,z})\sin(\tilde{u}_{1,z})\end{pmatrix}f_{z,1}$$
$$=\frac{W_c^2n_ca_c}{2}\Delta\delta\lambda_{des} \tag{46}$$

$$\left(\cos\left(Cu_{t_m}+(1-C)\widehat{u}_{1,y}\right)\sin\left((1-C)\tilde{u}_{1,y}\right)\right)f_{y,1}+\left(\cos\left(Cu_{t_m}\right.\right.$$
$$\left.\left.+(1-C)\widehat{u}_{2,y}\right)\sin\left((1-C)\tilde{u}_{2,y}\right)\right)f_{y,2}+\left(\cos\left(Cu_{t_m}\right.\right.$$
$$\left.\left.+(1-C)\widehat{u}_{3,y}\right)\sin\left((1-C)\tilde{u}_{3,y}\right)\right)f_{y,3}=\frac{(1-C)W_cn_ca_c}{4}\delta e_{x,des} \tag{47}$$

$$\begin{aligned}&\left(\sin\left(Cu_{t_m}+(1-C)\widehat{u}_{1,y}\right)\sin\left((1-C)\tilde{u}_{1,y}\right)\right)f_{y,1}+\left(\sin\left(Cu_{t_m}\right.\right.\\&\left.+(1-C)\widehat{u}_{2,y}\right)\sin\left((1-C)\tilde{u}_{2,y}\right)\Big)f_{y,2}+\left(\sin\left(Cu_{t_m}\right.\right.\\&\left.+(1-C)\widehat{u}_{3,y}\right)\sin\left((1-C)\tilde{u}_{3,y}\right)\Big)f_{y,3}\\&=\frac{(1-C)W_c n_c a_c}{4}\Delta\delta e_{y,des}\end{aligned}\tag{48}$$

$$\cos(\widehat{u}_{1,z})\sin(\tilde{u}_{1,z})f_{z,1}=\frac{W_c n_c a_c}{2}\Delta\delta i_{x,des}\tag{49}$$

$$\begin{aligned}&\left(7K_cS_c\left(u_{t_m}-\widehat{u}_{1,y}\right)\tilde{u}_{1,y}\right)f_{y,1}+\left(7K_cS_c\left(u_{t_m}-\widehat{u}_{2,y}\right)\tilde{u}_{2,y}\right)f_{y,2}+\left(7K_cS_c\left(u_{t_m}\right.\right.\\&\left.\left.-\widehat{u}_{3,y}\right)\tilde{u}_{3,y}\right)f_{y,3}+\begin{pmatrix}2K_cT_c(u_{t_m}-\widehat{u}_{1,z}-\tilde{u}_{1,z})\cos(\widehat{u}_{1,z})\sin(\tilde{u}_{1,z})+\\+(W_c+2K_cT_c)\sin(\widehat{u}_{1,z})\sin(\tilde{u}_{1,z})+\\-2K_cT_c\sin(\widehat{u}_{1,z}-\tilde{u}_{1,z})\tilde{u}_{1,z}\end{pmatrix}f_{z,1}\\&=\frac{W_c^2 n_c a_c}{2}\Delta\delta i_{y,des}\end{aligned}\tag{50}$$

The system (45)–(50) of 6 equations in 8 unknowns can be solved numerically using a nonlinear least-squares problem method [21]. In this work, the Levenberg-Marquardt algorithm [22] implemented in the *fsolve* Matlab routine is used. Note that the proposed numerical approach only guarantees the achievement of the desired relative configuration in a computationally efficient way. However, it does not enable the minimization of the fuel consumption. Ultimately, it is worth remarking that the obtained solution takes into account the dynamics coupling between the in-plane and out-of-plane motion.

4. Numerical validation of the control solutions

In this section the relative trajectories obtained using the developed control solutions are presented, pointing out their performances in terms of maneuver cost and accuracy. Fig. 2 illustrates the simulation setup exploited for the validation of the proposed maneuvering solutions.

First, the initial mean orbit elements of the chief and the mean ROE state are set. Then, the initial mean orbit elements of the deputy are computed using the identities in Eq. (8). A numerical propagator including the Earth's oblateness J_2 effects is used to obtain the history of position and velocity of chief and deputy spacecraft expressed in Earth Centered Inertial (ECI) reference frame (J2000). The initial Cartesian state of both satellites are derived using the linear mapping developed by Brouwer and Lyddane to transform the mean orbit elements into osculating and the nonlinear relations between Cartesian state and osculating elements [23–25]. The control thrust profile is projected into the ECI frame and added as external accelerations to the deputy's motion. Note that 100 (kg) class of spacecraft are considered in this work, equipped with cold gas propulsion system [26] for the relative maneuvering. After the simulation, the absolute position and velocity of the spacecraft are converted into the mean orbit elements to compute the accuracy at the end of the maneuvering interval, defined as

$$\varepsilon_{\delta\alpha_k}=\left|\delta\alpha_k^{num}(t_m)-\delta\alpha_{k,des}\right|a_c(t_0)\quad k=1,\ldots,6.\tag{51}$$

In order to verify the effectiveness of the continuous thrust maneuvers discussed in section 3, three test cases are carried out, involving the in-plane, out-of-plane, and full reconfiguration maneuvers defined in section 3.1. Moreover, a comparison with the corresponding impulsive control scheme reported in Ref. [3] is presented for in-plane and out-of-plane reconfiguration problems. A numerical optimizer is also used to verify the cost efficiency of the proposed solutions. However, it must be said that a detailed study of the optimality of the solution is not carried out in the frame of this work. The following minimum-fuel reconfiguration problems are investigated in the next sections:

- *In-plane minimum-fuel reconfiguration*. Find $f_{j,y}$, $\tilde{u}_{j,y}$ and $\widehat{u}_{j,y}$ with $j=1,\ldots,N_y$ that minimize $\Delta v_{TOT}=\sum_{j=1}^{N_y}2f_{y,j}\tilde{u}_{j,y}/W_c$ subject to

$$\begin{aligned}&\Delta\delta\widetilde{\boldsymbol{\alpha}}_{des}^{ip}=\boldsymbol{\varsigma}_y^{ip}\\&\left|f_{y,j}\right|<f_{max}^{ip},\quad \widehat{u}_{j+1,y}>\widehat{u}_{j,y},\quad \left|\tilde{u}_{j+1,y}+\tilde{u}_{j,y}\right|<\left|\widehat{u}_{j+1,y}-\widehat{u}_{j,y}\right|.\end{aligned}\tag{52}$$

- *Out-of-plane minimum-fuel reconfiguration*. Find $f_{j,z}$, $\tilde{u}_{j,z}$ and $\widehat{u}_{j,z}$ that minimize $\Delta v_{TOT}=\sum_{j=1}^{N_z}2f_{z,j}\tilde{u}_{j,z}/W_c$ subject to

$$\begin{aligned}&\Delta\delta\widetilde{\boldsymbol{\alpha}}_{des}^{oop}=\boldsymbol{\varsigma}_z^{oop}\\&\left|f_{z,j}\right|<f_{max}^{oop},\quad \widehat{u}_{j+1,z}>\widehat{u}_{j,z},\quad \left|\tilde{u}_{j+1,z}+\tilde{u}_{j,z}\right|<\left|\widehat{u}_{j+1,z}-\widehat{u}_{j,z}\right|.\end{aligned}\tag{53}$$

- *Full minimum-fuel reconfiguration*. Find $f_{j,y}$, $\tilde{u}_{j,y}$ and $\widehat{u}_{j,y}$ with $j=1,\ldots,N_y$, and $f_{j,z}$, $\tilde{u}_{j,z}$ and $\widehat{u}_{j,z}$ that minimize $\Delta v_{TOT}=\sum_{j=1}^{N_y}2f_{y,j}\tilde{u}_{j,y}/W_c+\sum_{j=1}^{N_z}2f_{z,j}\tilde{u}_{j,z}/W_c$ subject to

$$\begin{aligned}&\Delta\delta\widetilde{\boldsymbol{\alpha}}_{des}^{full}=\boldsymbol{\varsigma}_y+\boldsymbol{\varsigma}_z\\&\left|f_{y,j}\right|<f_{max}^{full},\quad \widehat{u}_{j+1,y}>\widehat{u}_{j,y},\quad \left|\tilde{u}_{j+1,y}+\tilde{u}_{j,y}\right|<\left|\widehat{u}_{j+1,y}-\widehat{u}_{j,y}\right|\\&\left|f_{z,j}\right|<f_{max}^{full},\quad \widehat{u}_{j+1,z}>\widehat{u}_{j,z},\quad \left|\tilde{u}_{j+1,z}+\tilde{u}_{j,z}\right|<\left|\widehat{u}_{j+1,z}-\widehat{u}_{j,z}\right|.\end{aligned}\tag{54}$$

where the term f_{max} in Eqs. (52)–(54) denotes the maximum available acceleration at the beginning of the maneuvering interval and ranges from $5\text{x}10^{-4}$ (m/s^2) for the in-plane simulated scenario to $5\text{x}10^{-3}$ (m/s^2) for the out-of-plane and full test cases. In this study, the global optimizer *MultiStart* provided by the Global Optimization Toolbox [27] is exploited to solve the above optimization problems. *MultiStart* implements stochastic search methods to find the global minimum. It uses multiple random start points (including the user-defined initial guess) to sample multiple basins of attraction and starts a local solver, such as *fmincon*, from those starting points, [28]. In the presented test cases 400 start points are used.

4.1. In-plane reconfiguration control problem

This section presents the trajectories obtained using the analytical

Table 1
Initial mean chief orbit.

a_c (km)	e_x (dim)	e_y (dim)	i_c (deg)	Ω_c (deg)	u_c (deg)
6578	0	0	8	0	0

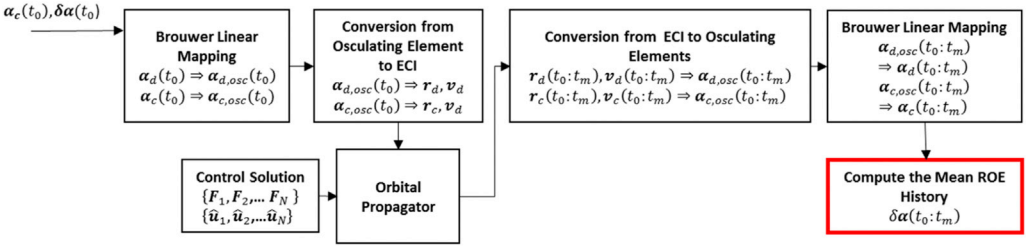

Fig. 2. Numerical validation scheme.

Table 2
Initial and desired relative orbit.

	$a_c\delta a$ (m)	$a_c\delta\lambda$ (m)	$a_c\delta e_x$ (m)	$a_c\delta e_y$ (m)	$a_c\delta i_x$ (m)	$a_c\delta i_y$ (m)
Initial relative orbit, $\delta\boldsymbol{\alpha}_0$	30	$-11e3$	0	-50	0	0
Desired relative orbit, $\delta\boldsymbol{\alpha}_{des}$	0	$-10.5e3$	45	70	–	–

control solution reported in Eqs. (38) and (39) and the numerical solution given by *MultiStart* solver. The initial conditions used in the simulations are listed in Tables 1 and 2 (see first row), along with the desired mean ROE vector. The initial mean state is expressed in terms of quasi-nonsingular orbital elements [17] in Table 1. Note that the values of $\delta\boldsymbol{\alpha}_0$ and $\delta\boldsymbol{\alpha}_{des}$ lead to

$$a_c\Delta\delta\widehat{\boldsymbol{\alpha}}_{des} = a_c\begin{bmatrix}\Delta\delta a_{des}\\ \Delta\delta\lambda_{des}\\ \Delta\delta e_{x,des}\\ \Delta\delta e_{y,des}\end{bmatrix} = [-0.03,\ 1.9172, 0.0403,\ 0.1198]^T\ (\text{km}). \quad (55)$$

The reconfiguration maneuver lasts 5 orbits, i.e. $u_f = 10\pi$ (rad), corresponding to $t_m = 439.92$ (min). In this simulation a maximum acceleration of $5e-4$ (m/s^2) is considered, compatible with the maximum thrust provided by the cold gas propulsion system [26]. The analytical solution is obtained by choosing the parameters $k = [k_1, k_2, k_3] = [0, 1, 6]$ (see Eq. (38)), corresponding to the maneuvers' locations, $\widehat{\bar{U}}_{j,y}$, listed in Table 3. This choice derive from the analysis conducted in Ref. [3], wherein an impulsive solution is computed considering three tangential impulses placed at the same instants. In addition, the analytical solution is computed assuming the maneuvers durations $\Delta t_y = [11.01,\ 22.02,\ 22.02]$ (min), corresponding to $\tilde{u}_{1,y} = \pi/4$ (rad) and $\tilde{u}_{2,y} = \tilde{u}_{2,y} = \pi/2$ (rad). The maneuvers' magnitudes given by Eq. (39) are $f_{y,1} = 1.865 \text{ x } 10^{-5}$ (m/s^2), $f_{y,2} = -3.774 \text{ x } 10^{-5}$ (m/s^2), and $f_{y,3} = 1.499 \text{ x } 10^{-5}$ (m/s^2) (see Fig. 3), corresponding to a total delta-V of 0.0820 (m/s). As discussed in previous section, the *MultiStart* solver allows the computation of the maneuvers' magnitudes, locations, and durations that minimize the total delta-V. As illustrated in Fig. 3 and confirmed by the results reported in Table 3, the numerical approach based on the global optimizer *MultiStart* reduces the maneuvers' durations and increases the maneuvers' magnitudes in order to decrease the fuel consumption. In further details, the *MultiStart* algorithm provides a control profile consisting of three maneuvers of magnitude $f_{y,1}^{MS} = -2.62 \text{ x } 10^{-4}$ (m/s^2), $f_{y,2}^{MS} = 3.563 \text{ x } 10^{-4}$ (m/s^2), and $f_{y,3}^{MS} = 4.509 \text{ x } 10^{-4}$ (m/s^2) and duration $\Delta t_y^{MS} = [2.94,\ 0.48,\ 0.67]$ (min), with a total maneuver cost of about 0.0749 m/s ($\Delta v_{TOT}^{MS} = 0.07489$ (m/s)). In other words, the *MultiStart* solution tends to the impulsive optimal one, decreasing the maneuver delta-V of 8.6% with respect to the analytical solution). It must be pointed out that the *MultiStart* approach provides better performance in terms of maneuver cost even when the maneuvers' durations are constrained to be equal to those chosen for the computation of the analytical solution, i.e. $\Delta t_y^{MS} = \Delta t_y = [11.01, 22.02, 22.02]$ (min). In this case, the *MultiStart* method provides a reconfiguration strategy requiring a delta-V of 0.0791 m/s (about the 3.5% lower than the delta-V required by the analytical solution), and consisting of three maneuvers of magnitude $f_{y,1}^{MS} = -0.7331 \text{ x } 10^{-4}$ (m/s^2), $f_{y,2}^{MS} = 0.1628 \text{ x } 10^{-4}$ (m/s^2), and $f_{y,3}^{MS} = 0.0694 \text{ x } 10^{-4}$ (m/s^2) placed at $\widehat{\bar{U}}_{1,y} = 4.356$ (rad), $\widehat{\bar{U}}_{2,y} = 7.5937$ (rad), and $\widehat{\bar{U}}_{3,y} = 26.4049$ (rad).

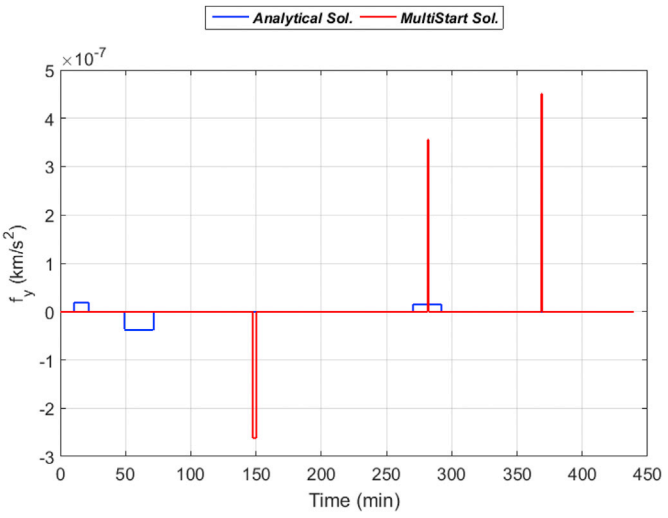

Fig. 3. Control profile for in-plane maneuver.

Figs. 4 and 5 illustrate the mean relative semi-major axis and longitude, and the x- and y-component of mean relative eccentricity vector respectively. Both osculating and mean ROE are shown in the same plots. From these figures, both analytical and minimum-fuel continuous control solutions guarantee the achievement of the desired in-plane conditions in the given interval of 5 orbits.

Table 4 shows the accuracy for the in-plane reconfiguration maneuvers, i.e. the difference between the mean ROE at the end of the maneuver, t_m, as computed by the numerical propagator, and the desired ROE multiplied by the chief mean-semi-major axis (see Eq. (51)). The final error is at the meter level and is mainly due to the approximations introduced by the osculating-to-mean transformation at the end of the simulations.

Ultimately, Fig. 6 shows the evolution of relative position in along-track/cross-track plane of chief RTN frame. In the same figure the finite-time maneuvers are depicted (see green markers). The initial and the desired relative positions are indicated by the cyan and black markers, respectively.

Table 3
Comparison between the analytical and numerical control solution for the in-plane maneuver.

	Man. Loc. $\widehat{\bar{U}}_{j,y}$ (rad)	$\Delta v_{j,y}$ (m/s)	Δv_{TOT} (m/s)
Analytical Continuous Solution	$\begin{bmatrix}1.245\\4.38\\20.09\end{bmatrix}$	$\begin{bmatrix}0.0123\\-0.0498\\0.0198\end{bmatrix}$	0.0820
Numerical Continuous Solution (*MultiStart*)	$\begin{bmatrix}10.67\\20.14\\26.34\end{bmatrix}$	$\begin{bmatrix}-0.0463\\0.0102\\0.0182\end{bmatrix}$	0.0749
Analytical Impulsive Solution ([3])	$\begin{bmatrix}1.245\\4.38\\20.09\end{bmatrix}$	$\begin{bmatrix}0.0092\\-0.0463\\0.0194\end{bmatrix}$	0.0748

4.2. Out-of-plane reconfiguration control problem

Here, the relative motion given by the cross-track maneuver presented in section 3.3 is shown. In this scenario, a maneuver lasting 7 orbits is considered, corresponding to $t_m = 655.2$ (min). The initial and desired states listed in Tables 5 and 6 are used to run the verification simulations. The values of $\delta\boldsymbol{\alpha}_0$ and $\delta\boldsymbol{\alpha}_{des}$ yield the following change of ROE

$$a_c\Delta\delta\widehat{\boldsymbol{\alpha}}_{des} = a_c\begin{bmatrix}\Delta\delta i_{x,des}\\ \Delta\delta i_{y,des}\end{bmatrix} = [0.3950,\ 0.0497]^T(\text{km}). \quad (56)$$

Eq. (43) is solved using the Brent's method [20] implemented in *fzero*

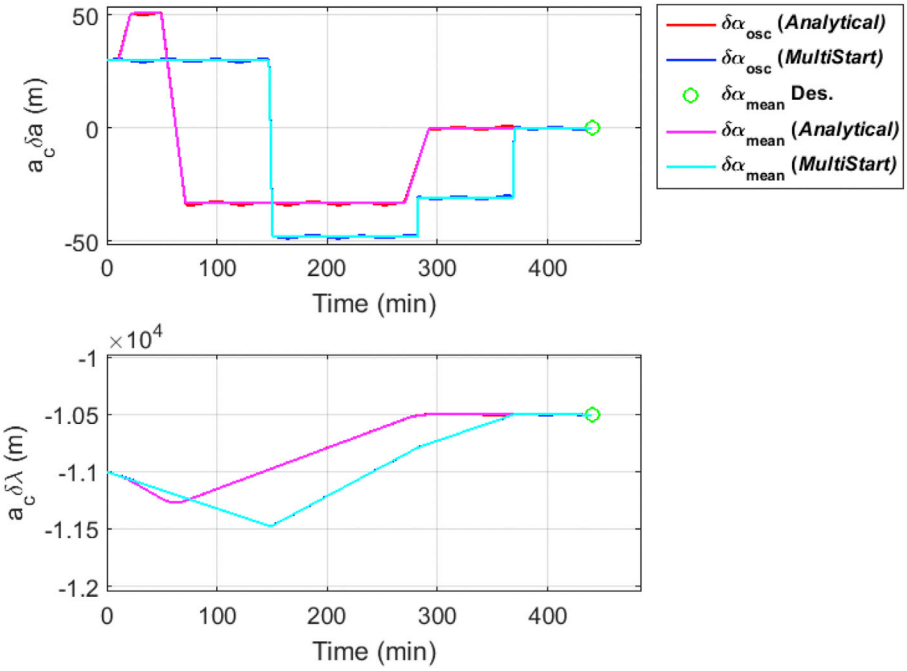

Fig. 4. Relative mean semi-major axis and longitude due to in-plane reconfiguration maneuver.

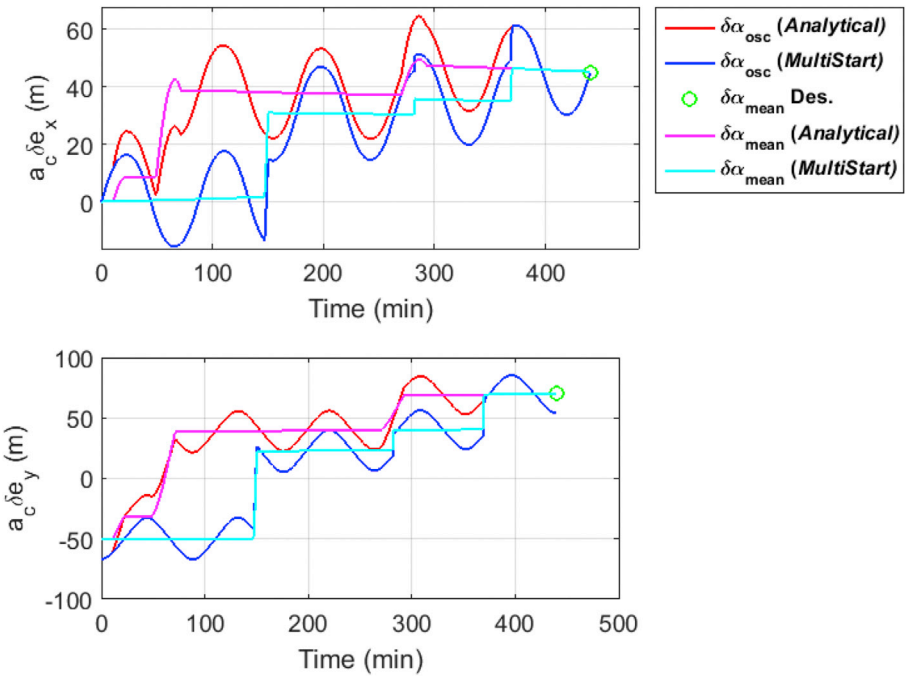

Fig. 5. x- and y-component of mean relative eccentricity vector due to in-plane reconfiguration maneuver.

Table 4
Accuracy of control solutions for in-plane maneuver.

	$\varepsilon_{\delta a}$ (m)	$\varepsilon_{\delta\lambda}$ (m)	$\varepsilon_{\delta e_x}$ (m)	$\varepsilon_{\delta e_y}$ (m)
Analytical Continuous Solution	0.0449	2.182	0.197	0.034
Numerical Continuous Solution	0.0451	2.187	0.192	0.035

Matlab routine (referred to as semi-analytical continuous solution from now on). It is worth remarking that a parametric analysis of the error function, J (see Eq. (44)), is carried out to determine a good initial guess for the "*fzero*" solver. Differently, the author of [3] used the closed-form control solution for unperturbed orbit as initial guess for the iterative algorithm, i.e. $\hat{u}_{1,z} = \text{atan}(\Delta i_{y,des}/\Delta i_{x,des})$. The semi-analytical solution is computed setting a maneuver duration of about 23 (min) (corresponding to $\tilde{u}_{1,z} = \pi/2$ (rad)) and provides a control profile made of a maneuver of magnitude $f_{z,1} = 3.505 \text{ x } 10^{-4}$ (m/s^2) located at $\hat{u}_{1,z} = 12.649$ (rad) (see Table 7), corresponding to a total delta-V of 0.492 m/s. The Brent's algorithm converges after 8 iterations. Table 7 shows also the maneuver location and the delta-V associated to the continuous solution given by the *MultiStart* solver and to the semi-analytical impulsive solution computed in Ref. [3]. The numerical approach based on the *MultiStart* tends to decrease the maneuver duration and increase the magnitude.

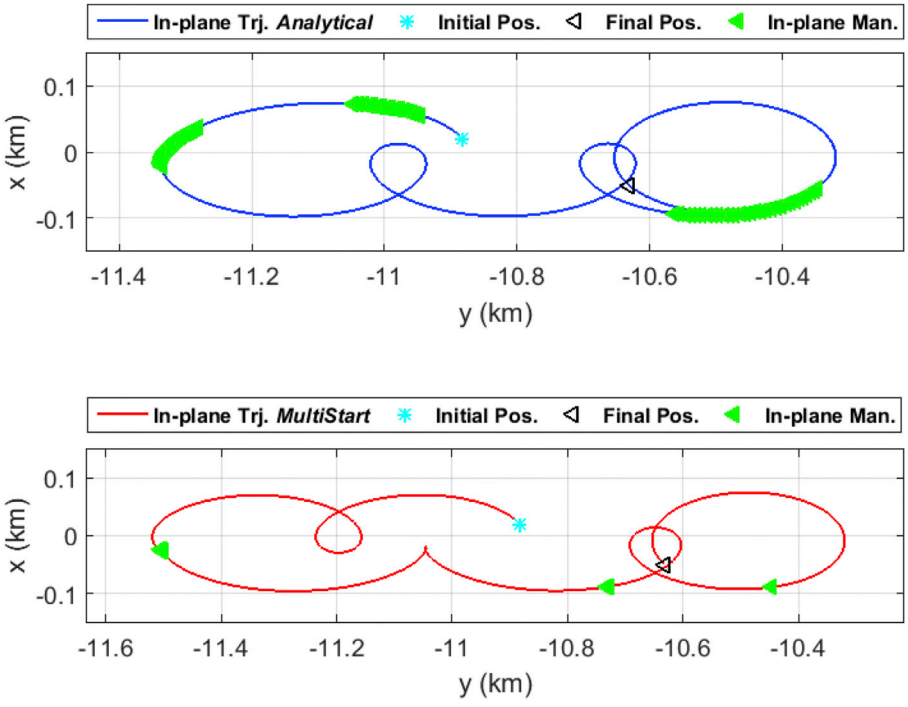

Fig. 6. Relative orbit projected on *x-y* plane of chief RTN frame.

Table 5
Initial mean chief orbit.

a_c (km)	e_x (dim)	e_y (dim)	i_c (deg)	Ω_c (deg)	u_c (deg)
6828	0	0	78	0	0

Table 6
Initial and desired relative orbit.

	$a_c\delta a$ (m)	$a_c\delta\lambda$ (m)	$a_c\delta e_x$ (m)	$a_c\delta e_y$ (m)	$a_c\delta i_x$ (m)	$a_c\delta i_y$ (m)
Initial relative orbit, $\delta\boldsymbol{\alpha}_0$	0	0	0	− 50	5	70
Desired relative orbit, $\delta\boldsymbol{\alpha}_{des}$	–	–	–	–	400	120

Table 7
Comparison between the semi-analytical and numerical control solutions for the out-of-plane maneuver.

	Man. Loc. $\hat{u}_{1,z}$ (rad)	$\Delta v_{1,z}$ (m/s)	Δv_{TOT} (m/s)
Semi-analytical Continuous Solution (*fzero*)	12.649	0.492	0.492
Numerical Continuous Solution (*MultiStart*)	0.0661	0.443	0.443
Semi-analytical Impulsive Solution ([3])	0.1275	0.443	0.443

More specifically, the *MultiStart* solver gives an extremal solution, i.e. $f_{z,1}^{MS} = f_{max} = 5 \times 10^{-3}$ (m/s^2), consisting of a maneuver of 1.47 (min) located at the beginning of the maneuvering interval (see Fig. 7). Note that the continuous semi-analytical solution is employed to initialize the *MultiStart* optimizer in this simulation. As expected, the *MultiStart* method reduces the total maneuver delta-V with respect to the

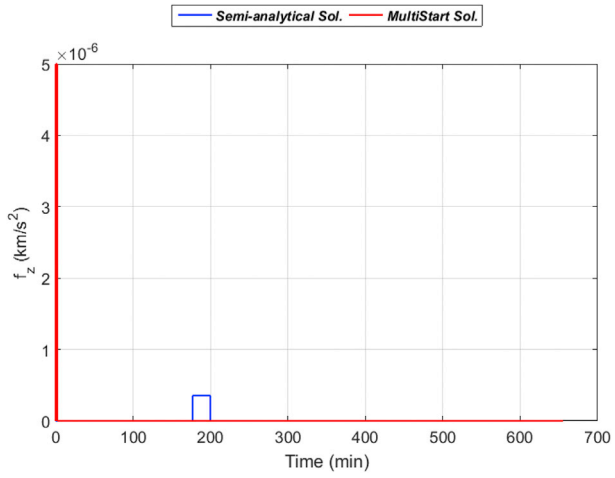

Fig. 7. Control profile for out-of-plane maneuver.

semi-analytical solution of about 12%, achieving the fuel consumption obtained by the optimal impulsive solution (see Table 7). However, when the maneuver duration is constrained to be equal to 23 (min), i.e. to the value set for the computation of the semi-analytical solution, the *MultiStart* solver does not provide an improvement in terms of delta-V, i.e. $\Delta v_{TOT}^{MS} = 0.492$ (m/s), even though the cross-track maneuver has a different position and magnitude ($f_{z,1}^{MS} = -3.5019 \times 10^{-4}$ (m/s^2) and $\hat{u}_{1,z}^{MS} = 3.2119$ (rad)).

Fig. 8 shows the change of mean and osculating relative vector over the maneuvering interval. Accordingly, both the continuous semi-analytical solution and the numerical one given by the *MultiStart* solver allow the achievement of the desired formation configuration within the 7 orbits maneuvering interval. Table 8 reports the accuracy at the end of the maneuvering interval for the designed out-of-plane maneuver. Here,

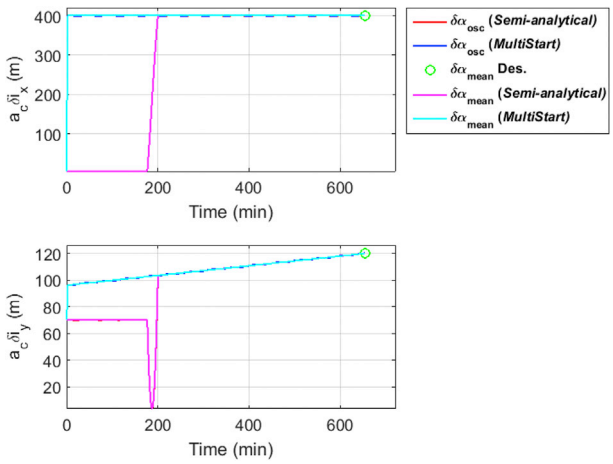

Fig. 8. x- and y-component of mean relative inclination vector due to out-of-plane maneuver.

Table 8
Accuracy of the control solutions for the out-of-plane maneuver.

	$\varepsilon_{\delta i_x}$ (m)	$\varepsilon_{\delta i_y}$ (m)
Semi-analytical Continuous Solution (*fzero*)	0.3014	0.0134
Numerical Continuous Solution (*MultiStart*)	0.3555	0.0165

the final error is at the centimeter level at most.

Fig. 9 illustrates the trajectory projected on the cross-track/radial plane of the chief RTN reference frame, along with its location. The initial and the aimed relative positions are indicated by the cyan and black markers, respectively.

4.3. Full reconfiguration control problem

In this section the full reconfiguration results are discussed. Here, a maneuver interval of 7 orbits is considered, i.e. $u_f = 14\pi$ (rad). Tables 9 and 10 report the initial and desired mean ROE respectively. In this scenario, a simple analytical solution cannot be computed, as discussed in section 3.4. Consequently, the Matlab built-in routine *fsolve* is used to derive the continuous control solution, i.e. to solve the nonlinear system of equations (45–(50) with respect to the variables $\hat{u}_{1,z}$, $f_{z,1}$, $\hat{u}_{1,y}$, $\hat{u}_{2,y}$, $\hat{u}_{3,y}$, and $f_{y,j}$ with $j = 1, \ldots, 3$. It is worth recalling that the *fsolve* solver does not minimize the fuel consumption but only guarantees the achievement of the desired relative conditions. As discussed in section 3.4, the maneuvers' durations are known parameters and, in this studied case, they are set equal to $\Delta t_y = [11.01, 22.03, 22.03]$ (min) (corresponding to $\tilde{u}_{1,y} = \pi/4$ (rad), $\tilde{u}_{2,y} = \tilde{u}_{2,y} = \pi/2$ (rad)) and $\Delta t_z = 22.03$ (min) (corresponding to $\tilde{u}_{1,z} = \pi/2$ (rad)) for tangential and cross-track maneuvers, respectively. The position of the second and third along-track maneuvers are enforced to have the form $\hat{u}_{2,y} = \hat{u}_{1,y} + k_2\pi/(1-C)$ and $\hat{u}_{3,y} = \hat{u}_{1,y} + k_3\pi/(1-C)$, being $k_2 = 1$ and $k_3 = 6$ integer numbers. This allows reducing the numbers of variables to 6.

Table 9
Initial mean chief orbit.

a_c (km)	e_x (dim)	e_y (dim)	i_c (deg)	Ω_c (deg)	u_c (deg)
6578	0	0	20	0	0

Table 10
Initial and desired relative orbit.

	$a_c\delta a$ (m)	$a_c\delta\lambda$ (m)	$a_c\delta e_x$ (m)	$a_c\delta e_y$ (m)	$a_c\delta i_x$ (m)	$a_c\delta i_y$ (m)
Initial relative orbit, $\delta\alpha_0$	30	− 11*e*3	0	− 0.05	5	70
Desired relative orbit, $\delta\alpha_{des}$	0	− 10.5*e*3	45	70	400	120

Table 11 reports the maneuvers' locations and cost obtained using both numerical approaches. The *fsolve* solver provides three tangential maneuvers of magnitude $f_{y,1} = 0.1716 \times 10^{-4}$ (m/s^2), $f_{y,2} = -0.3765 \times 10^{-4}$ (m/s^2), and $f_{y,3} = 0.1564 \times 10^{-5}$ (m/s^2) and a single cross-

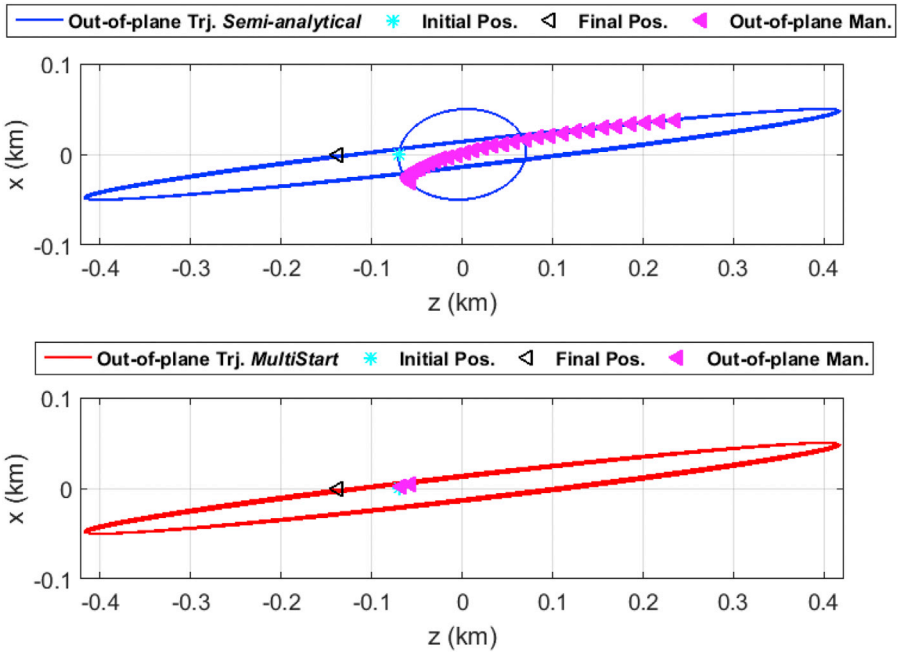

Fig. 9. Relative orbit projected on x-z plane of RTN frame.

Table 11
Comparison between the two numerical control solutions for out-of-plane maneuver.

	Man. Loc.$\hat{u}_{j,y}$ (rad)	Man. Loc. $\hat{u}_{1,z}$ (rad)	$\Delta v_{j,y}$ (m/s)	$\Delta v_{1,z}$ (m/s)	Δv_{TOT} (m/s)
fsolve Continuous Solution	$\begin{bmatrix}1.142\\4.29\\20.04\end{bmatrix}$	12.68	$\begin{bmatrix}0.0113\\-0.0497\\0.0206\end{bmatrix}$	0.523	0.604
Multistart Continuous Solution	$\begin{bmatrix}4.279\\32.659\\42.078\end{bmatrix}$	31.54	$\begin{bmatrix}-0.0322\\0.0285\\-0.0140\end{bmatrix}$	0.427	0.546

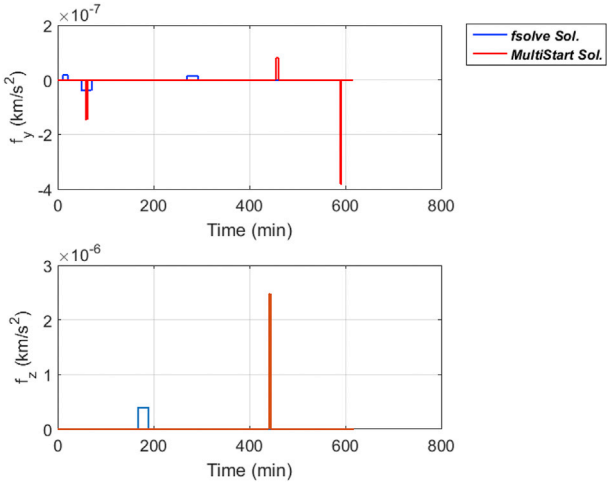

Fig. 10. Control profile for full reconfiguration maneuver.

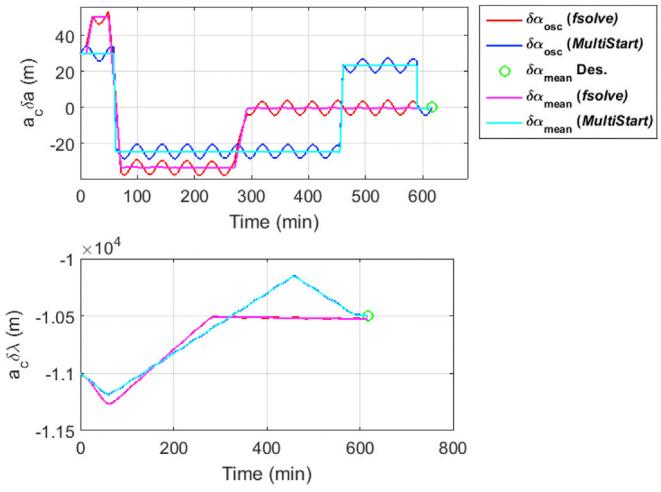

Fig. 11. Relative mean semi-major axis and longitude due to full reconfiguration maneuver.

track maneuver of magnitude $f_{z,1} = 3.955 \times 10^{-4}$ (m/s^2), with a total delta-V of 0.604 (m/s) (see Fig. 10). As can be seen, *MultiStart*-based approach produces an improvement of 6.6% in terms of delta-V with respect to the *fsolve* solution. Again, the optimizer tends to reduce the maneuvers' duration and raise the magnitudes to decrease the delta-V. However, the obtained minimum-fuel solution is not extremal, i.e. $|f_{y,j}|$ with $j = 1, \ldots, 3$ and $|f_{z,1}|$ are lower than the maximum value $f_{max} =$ $5\text{x}10^{-3}$ (m/s^2). It is worth remarking that the numerical continuous solution obtained through the *fsolve* routine is exploited as initial guess of *MultiStart* solver.

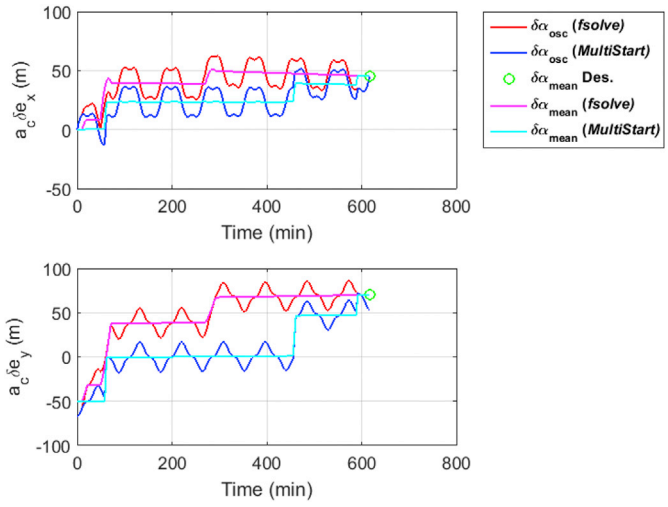

Fig. 12. x- and y-component of mean relative eccentricity vector due to full reconfiguration maneuver.

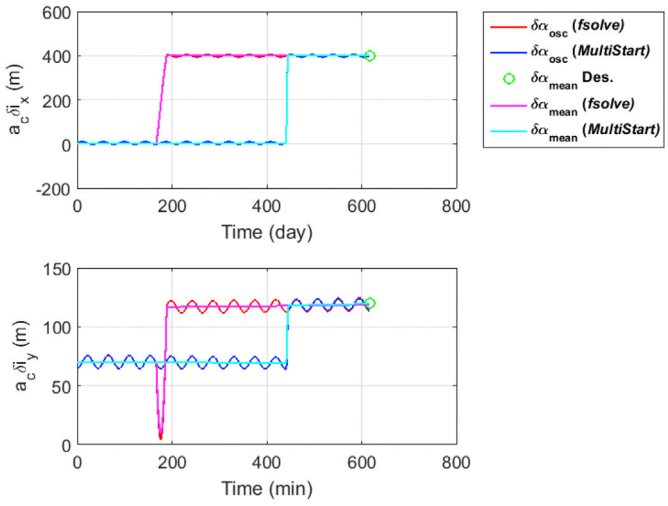

Fig. 13. x- and y-component of mean relative inclination vector due to full reconfiguration maneuver.

Figs. 11–13 illustrate the variation of the mean and osculating ROE over the time, whereas Fig. 10 shows the component x and z of the control thrust vector given by the two employed numerical approaches. From these figures, both numerical approaches guarantee the achievement of the desired formation configuration within the maneuvering interval of 7 orbits.

Figs. 14 and 15 illustrate the relative orbit projected on radial/along-track and radial/cross-track planes of chief RTN frame, respectively. From these plots, the dynamical coupling between the in-plane and out-of-plane motion can be clearly observed. Thus, with reference to Fig. 15, the out-of-plane trajectory is modified by the along-track maneuvers (green markers).

Finally, Table 12 summarizes the accuracy of the designed maneuvers. Here it is shown that the proposed maneuvering scheme controls the mean relative longitude with comparatively coarse accuracy

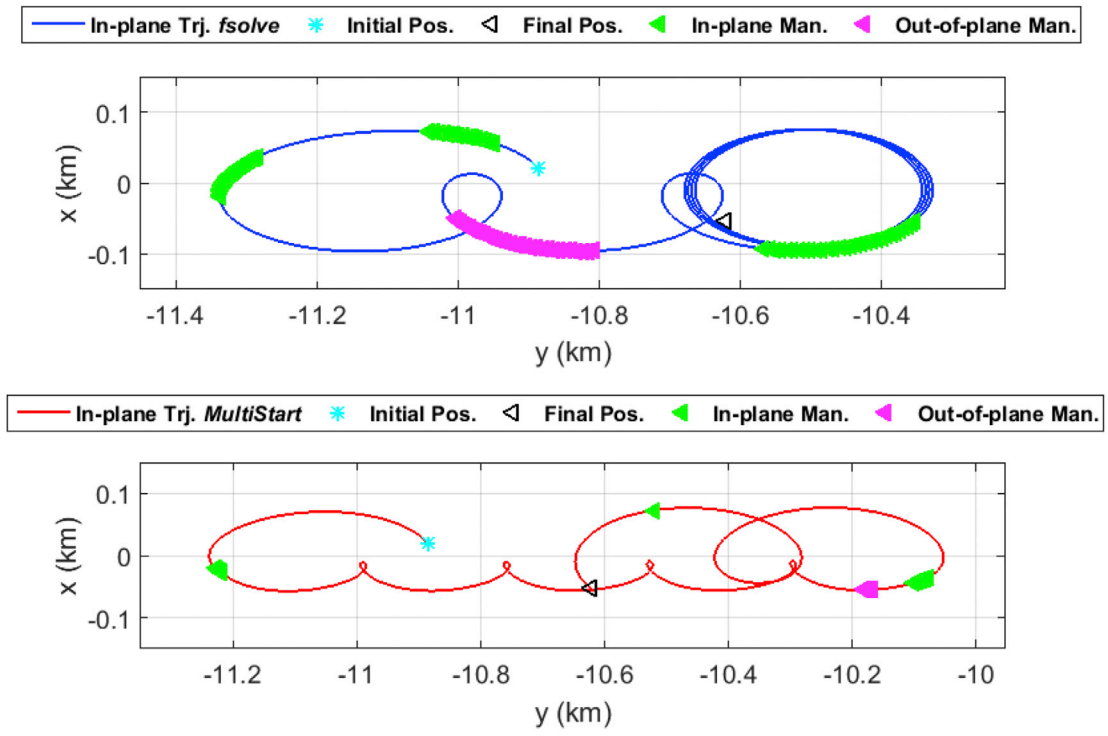

Fig. 14. Relative orbit projected on *x-y* plane of RTN frame.

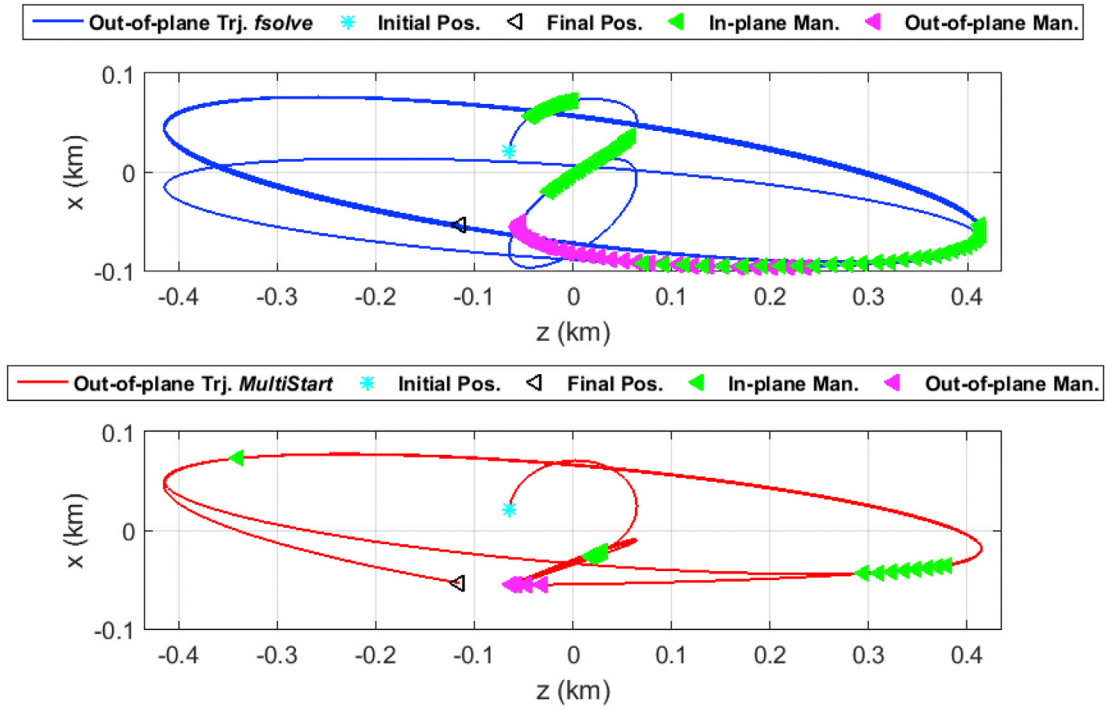

Fig. 15. Relative orbit projected on *x-z* plane of RTN frame.

($\varepsilon_{\delta\lambda}^{fsolve} = 17$ m, $\varepsilon_{\delta\lambda}^{MS} = 6$ m). However, the errors on the other components of final ROE vector remain small (at the centimeter level).

Note that the full formation reconfiguration might be achieved by combining the solutions detailed in sections 3.2 and 3.3. However, considering the cross-track and along-track maneuvers separately doesn't account for the dynamics coupling between the out-of-plane and in-plane relative motions. For the sake of the example, let us assume to tackle the same full reconfiguration problem here studied by solving separately the in-plane and out-of-plane reconfiguration problems using the analytical and semi-analytical methods described in sections 3.2 and 3.3 respectively. Table 13 shows the maneuvers' location and magnitudes as well as the corresponding delta-V, assuming the maneuvers' durations are the same chosen to determine the maneuvering strategy through the fsolve-based approach. In this case, a decrease of the relative longitude and

Table 12
Accuracy of control solutions for full maneuver.

	$\varepsilon_{\delta a}$ (m)	$\varepsilon_{\delta\lambda}$ (m)	$\varepsilon_{\delta e_x}$ (m)	$\varepsilon_{\delta e_y}$ (m)	$\varepsilon_{\delta i_x}$ (m)	$\varepsilon_{\delta i_y}$ (m)
fsolve Continuous Solution	0.349	17.13	0.444	0.060	0.683	0.689
Multistart Continuous Solution	0.348	6.21	0.423	0.056	0.696	0.528

Table 13
Separately computed in-plane and out-of-plane solutions for the full-reconfiguration maneuver.

	Man. Loc. (rad)	Man. Δv(m/s)	Man. Magnitudex10^{-4} (m/s^2)	Δv_{TOT} (m/s)
In-plane Solution (*analytical*)	$\hat{u}_y = \begin{bmatrix} 1.142 \\ 4.292 \\ 20.040 \end{bmatrix}$	$\Delta v_y = \begin{bmatrix} 0.012 \\ -0.049 \\ 0.0197 \end{bmatrix}$	$f_y = \begin{bmatrix} 0.1847 \\ -0.376 \\ 0.149 \end{bmatrix}$	0.0817
Out-of-plane Solution (*fzero*)	$\hat{u}_{1,z} =$ 12.68	$\Delta v_{1,z} =$ 0.522	$f_{z,1} = 3.955$	0.522

relative inclination accuracies could be observed, i.e. $\varepsilon_{\delta\lambda}^{ip/oop} = 25.89$ (m) and $\varepsilon_{\delta i_y}^{ip/oop} = 1.25$ (m), even though the total maneuver cost remains the same, i.e. $\Delta v_{TOT}^{ip/oop} = 0.0817 + 0522 = 0.604$ (m/s).

4.4. Accuracy comparison between continuous and impulsive approaches

The impulsive scheme implies an instantaneous variation of the deputy velocity with no change of position, i.e. an instantaneous change of mean ROE ([3]). In fact, an impulsive maneuver is only a mathematical model that doesn't allow accounting for the effects due to finite duration thrust on the relative dynamics. In light of this, the impulsive approach can be adopted only when the firing interval is small as compared with the orbital period, otherwise it might fail in achieving the desired level of accuracy. Many real applications might require a long time maneuver in order to meet some specific constraints, e.g. the maximum thrust provided by onboard actuators. The proposed continuous approach overcomes this problem by including the input matrix, $\boldsymbol{B}_{NC}$, in the derivation of control solution. To show the increased maneuver accuracy of the continuous approach over the impulsive one, let consider the same scenario described in section 4.1 (see Tables 1 and 2). Without loss of generality, the in-plane reconfiguration is assumed to be performed by three tangential maneuvers located at $\widehat{U}_{j,y} = [4.39, 16.96, 26.38]$ (rad) (i.e., $k = [k_1, k_2, k_3] = [1, 4, 7]$). Note that the instantaneous velocity change computed by the impulsive approach is transformed into a constant acceleration dividing the delta-V by firing duration, i.e.

$$f_{y,j}^{imp} = \frac{\Delta v_{y,j}^{imp}}{\Delta t_{j,y}} = \frac{\Delta v_{y,j}^{imp} W_c}{2\tilde{u}_{y,j}}, \quad j = 1, \ldots 3\,. \tag{57}$$

Here, the maneuver durations are $\Delta t_y = [22.02, 44.04, 66.07]$ (min), corresponding to $\tilde{u}_y = \left[\frac{\pi}{2}, \pi, \frac{3}{4}\pi\right]$ (rad). Table 14 reports the reconfiguration accuracy as defined in Eq. (51) for both continuous and impulsive schemes. As can be seen, the impulsive strategy produces a high error on the final relative eccentricity ($\varepsilon_{\delta e} = \sqrt{\varepsilon_{\delta e_x}^2 + \varepsilon_{\delta e_y}^2} = 53.55$ m), whereas it provides the same accuracy level on the mean semi-major axis and longitude. In fact, the equations describing the variation of δe_x and δe_y (29)–(30) are nonlinear in terms of parameter $\tilde{u}_{j,y}$ with $j = 1, \ldots 3$. Since

Table 14
Accuracy of control solutions for out-of-plane maneuver.

	$\varepsilon_{\delta a}$ (m)	$\varepsilon_{\delta\lambda}$ (m)	$\varepsilon_{\delta e_x}$ (m)	$\varepsilon_{\delta e_y}$ (m)
Continuous Solution	0.045	2.459	0.189	0.039
Impulsive Solution	0.047	2.474	16.665	50.901

the mapping between the continuous thrust $f_{y,j}^{imp}$ and the impulse $\Delta v_{y,j}^{imp}$ is linear, substituting Eq. (57) into Eqs. (29) and (30) doesn't cancel the parameter $\tilde{u}_{j,y}$. Hence, the relationships obtained by imposing Eq. (57) to Eqs. (29) and (30) do not match the corresponding equations of impulsive model reported in Ref. [3]. However, the above linear map allows reducing Eqs. (27) and (28) to the corresponding equations obtained by the impulsive scheme.

Finally, it is noteworthy that when the firing duration decreases the accuracies of continuous and impulsive solutions tend to be the same. In fact, $\sin(\tilde{u}_{j,y}) \approx \tilde{u}_{j,y}$ when $\tilde{u}_{j,y} \to 0$ (i.e., $\Delta t_{j,y} \to 0$), reducing Eqs. (27) and (28) to the corresponding impulsive equations.

5. Conclusion

This paper addressed the computation of control solutions for spacecraft formation reconfiguration problems using finite-time maneuvers. A fully analytical solution for in-plane reconfiguration maneuvers was derived by inverting the relative orbit element-based linearized equations of relative motion and considering three tangential maneuvers. A semi-analytical approach was proposed for out-of-plane relative motion control with a single maneuver. In addition, a solution for the full reconfiguration problem was numerically computed taking advantages of the results obtained for the in-plane and out-of-plane problems. A minimum-fuel solution was also derived for in-plane, out-of-plane, and full reconfiguration problems using a global optimization algorithm.

Numerical simulations showed the performances of the proposed control schemes in terms of maneuver cost and accuracy. The analytical and semi-analytical solutions derived for the in-plane and out-of-plane problems, respectively, guarantee a final accuracy at the centimeter level, whereas the numerical solution derived for the full reconfiguration problem provides an accuracy at the meter level. In addition, the iterative algorithms used for solving the out-of-plane and full reconfiguration problems could be easily implemented onboard given their proven fast convergence capability (at most 11 iterations). The main drawback of the proposed approaches is that they only allow finding a feasible maneuvering strategy, i.e. only guarantee the achievement of the desired final relative configuration. In other words, they do not enable the minimization of the maneuvering cost. The results presented in this paper, however, showed that the maximum increase of 12% of the total delta-V with respect to the corresponding minimum-fuel solution can be reached.

Finally, the results showed that the use of a dynamics model taking into account the dynamical effects of a continuous control acceleration enables increasing the accuracy of the maneuver, with respect to the impulsive strategy. More specifically, for the studied scenario it turned out that the use of the developed linear dynamics model improves the accuracy on the mean relative eccentricity vector.

Future work on the topic will include a thorough optimality assessment of the solutions derived in this work, as well as the extension of the continuous scheme to orbits of arbitrary eccentricity.

Acknowledgments

The authors would like to thank the United States Air Force Research Laboratory, Space Vehicles Directorate, for sponsoring this investigation under contract FAA9453-16-C-0029.

Appendix A. Control influence matrix Γ

The elements of control influence matrix $\mathbf{\Gamma}_F$ (see Eq. (6)) are

$$
\begin{aligned}
&\gamma_{13} = \gamma_{51} = \gamma_{52} = \gamma_{61} = \gamma_{62} = 0 \\
&\gamma_{11} = \frac{2e_d s_{f_d}}{n_d \eta_d a_c} \quad \gamma_{12} = \frac{2\left(1 + e_d c_{f_d}\right)}{n_d \eta_d a_c} \\
&\gamma_{21} = -\frac{\eta_d e_d c_{f_d}}{a_d n_d (1 + \eta_d)} - \frac{2\eta_d^2}{a_d n_d \left(1 + e_d c_{f_d}\right)} \\
&\gamma_{22} = -\frac{\eta_d e_d \left[\left(2 + e_d c_{f_d}\right) s_{f_d}\right]}{a_d n_d (1 + \eta_d)\left(1 + e_d c_{f_d}\right)} \quad \gamma_{23} = -\frac{\eta s_{\theta_d}\left(c_{i_c} - c_{i_d}\right)}{a_d n_d \left(1 + e_d c_{f_d}\right) s_{i_d}} \\
&\gamma_{31} = \frac{\eta_d s_{\theta_d}}{a_d n_d} \quad \gamma_{32} = \frac{\eta_d \left(2 + e_d c_{f_d}\right) c_{\theta_d} + \eta_d e_{x,d}}{a_d n_d \left(1 + e_d c_{f_d}\right)} \\
&\gamma_{33} = \frac{\eta_d e_{y,d} s_{\theta_d} cotg(i_d)}{a_d n_d \left(1 + e_d c_{f_d}\right)} \quad \gamma_{41} = -\frac{\eta_d c_{\theta_d}}{a_d n_d} \\
&\gamma_{42} = \frac{\eta_d \left(2 + e_d c_{f_d}\right) s_{\theta_d} + \eta_d e_{y,d}}{a_d n_d \left(1 + e_d c_{f_d}\right)}, \quad \gamma_{43} = -\frac{\eta_d e_{x,d} s_{\theta_d} cotg(i_d)}{a_d n_d \left(1 + e_d c_{f_d}\right)} \\
&\gamma_{53} = \frac{\eta_d s_{\theta_d}}{a_d n_d \left(1 + e_d c_{f_d}\right)} \quad \gamma_{63} = \frac{\eta_d c_{\theta_d} s_{i_c}}{a_d n_d \left(1 + e_d c_{f_d}\right) s_{i_d}}
\end{aligned}
\tag{A.1}
$$

where f_d and θ_d represent the deputy satellite's true anomaly and true argument of latitude respectively, and $e_{x,d} = e_d \cos(\omega_d)$ and $e_{y,d} = e_d \sin(\omega_d)$. The symbols $s_{(.)}$ and $c_{(.)}$ denote the $\sin(.)$ and $\cos(.)$ functions respectively.

Appendix B. In-plane reconfiguration

This appendix details the quantities Ξ_j with $j = 1, \ldots 3$ and D needed to compute the analytical solution for the in-plane reconfiguration (see Eq. (39)).

$$
\begin{aligned}
\Xi_1 &= (-1)^{k_1}(-1)^{k_2}\Lambda_c \widetilde{\overline{U}}_{3,y} \sin\left(\widetilde{\overline{U}}_{2,y}\right)\left(u_{t_m} - \widehat{\overline{U}}_{3,y}\right)\Delta\delta a_{des} + \\
&= -(-1)^{k_1}(-1)^{k_3}\Lambda_c \widetilde{\overline{U}}_{2,y} \sin\left(\widetilde{\overline{U}}_{3,y}\right)\left(u_{t_m} - \widehat{\overline{U}}_{2,y}\right)\Delta\delta a_{des} + \\
&= -\pi\Lambda_c \Delta\delta e_{des}(k_2 - k_3)\widetilde{\overline{U}}_{2,y}\widetilde{\overline{U}}_{3,y} + \\
&= +(-1)^{k_1}(-1)^{k_2}(1 - C)W_c \widetilde{\overline{U}}_{3,y} \sin\left(\widetilde{\overline{U}}_{2,y}\right)\Delta\lambda_{des} + \\
&= -(-1)^{k_1}(-1)^{k_3}(1 - C)W_c \widetilde{\overline{U}}_{2,y} \sin\left(\widetilde{\overline{U}}_{3,y}\right)\Delta\lambda_{des}
\end{aligned}
\tag{B.1}
$$

$$
\begin{aligned}
\Xi_2 &= (-1)^{k_1}\Lambda_c \widetilde{\overline{U}}_{3,y} \sin\left(\widetilde{\overline{U}}_{1,y}\right)\left(u_{t_m} - \widehat{\overline{U}}_{3,y}\right)\Delta\delta a_{des} + \\
&= -(-1)^{k_1}(-1)^{k_3}\Lambda_c \widetilde{\overline{U}}_{1,y} \sin\left(\widetilde{\overline{U}}_{3,y}\right)\left(u_{t_m} - \widehat{\overline{U}}_{1,y}\right)\Delta\delta a_{des} + \\
&= +\pi\Lambda_c(k_3)\widetilde{\overline{U}}_{1,y}\widetilde{\overline{U}}_{3,y}\Delta\delta e_{des} + \\
&= +(-1)^{k_1}(1 - C)W_c \widetilde{\overline{U}}_{3,y} \sin\left(\widetilde{\overline{U}}_{1,y}\right)\Delta\lambda_{des} + \\
&= -(-1)^{k_1}(-1)^{k_3}(1 - C)W_c \widetilde{\overline{U}}_{1,y} \sin\left(\widetilde{\overline{U}}_{3,y}\right)\Delta\lambda_{des}
\end{aligned}
\tag{B.2}
$$

$$
\begin{aligned}
\Xi_3 &= (-1)^{k_1}\Lambda_c \widetilde{\overline{U}}_{2,y} \sin\left(\widetilde{\overline{U}}_{1,y}\right)\left(u_{t_m} - \widehat{\overline{U}}_{2,y}\right)\Delta\delta a_{des} + \\
&= -(-1)^{k_1}(-1)^{k_2}\Lambda_c \widetilde{\overline{U}}_{1,y} \sin\left(\widetilde{\overline{U}}_{2,y}\right)\left(u_{t_m} - \widehat{\overline{U}}_{1,y}\right)\Delta\delta a_{des} + \\
&= +\pi\Lambda_c(k_2)\widetilde{\overline{U}}_{1,y}\widetilde{\overline{U}}_{2,y}\Delta\delta e_{des} + \\
&= +(-1)^{k_1}(1 - C)W_c \widetilde{\overline{U}}_{2,y} \sin\left(\widetilde{\overline{U}}_{1,y}\right)\Delta\lambda_{des} + \\
&= -(-1)^{k_1}(-1)^{k_2}(1 - C)W_c \widetilde{\overline{U}}_{1,y} \sin\left(\widetilde{\overline{U}}_{2,y}\right)\Delta\lambda_{des}
\end{aligned}
\tag{B.3}
$$

$$D = 4\pi\Lambda_c \left[\widetilde{\overline{U}}_{2,y} \widetilde{\overline{U}}_{3,y} \sin\left(\widetilde{\overline{U}}_{1,y}\right)(k_2 - k_3) + (-1)^{k_2} \widetilde{\overline{U}}_{1,y} \widetilde{\overline{U}}_{3,y} k_3 \right.$$
$$\left. D = (-1)^{k_2} \widetilde{\overline{U}}_{1,y} \widetilde{\overline{U}}_{3,y} k_3 \sin\left(\widetilde{\overline{U}}_{2,y}\right) - (-1)^{k_3} \widetilde{\overline{U}}_{1,y} \widetilde{\overline{U}}_{2,y} k_2 \sin\left(\widetilde{\overline{U}}_{3,y}\right) \right] \tag{B.4}$$

where

$$\Delta\delta e_{des} = \sqrt{\Delta\delta e_x^2 + \Delta\delta e_y^2}. \tag{B.5}$$

References

[1] S. Vaddi, K. Alfriend, S. Vadali, P. Sengupta, Formation establishment and reconfiguration using impulsive control, J. Guid. Contr. Dynam. 28 (no. 2) (2005) 262–268, https://doi.org/10.2514/1.6687.

[2] Y. Ichimura, A. Ichikawa, Optimal impulsive relative orbit transfer along a circular orbit, J. Guid. Contr. Dynam. 31 (no. 4) (2008) 1014–1027, https://doi.org/10.2514/1.32820.

[3] M. Chernick and S. D'Amico, "New Closed-form Solutions for Optimal Impulsive Control of Spacecraft Relative Motion," AIAA Space and Astronautics Form and Exposition, SPACE 2016, Long Beach Convention Center California.

[4] M. Lawn, G. Di Mauro and R. Bevilacqua, "Guidance solutions for spacecraft planar rephasing and rendezvous," 27th AAS/AIAA Space Flight Mechanics Meeting, San Antonio, Texas, February 5-9, 2017.

[5] L. Steindorf, S. D'Amico, J. Scharnagl, F. Kempf and K. Schilling, "Constrained low-thrust satellite formation-flying using relative orbit elements," 27th AAS/AIAA Space Flight Mechanics Meeting, San Antonio, Texas, February 5–9.

[6] A. Richards, T. Schouwenaars, J.P. How, E. Feron, Spacecraft trajectory planning with avoidance constraints using mixed-integer linear programming, J. Guid. Contr. Dynam. 25 (4) (2002) 755–764, https://doi.org/10.2514/2.4943.

[7] G.T. Huntington, A.V. Rao, Optimal reconfiguration of spacecraft formations using the Gauss pseudospectral meth-od, J. Guid. Contr. Dynam. 31 (3) (2008) 689–698, https://doi.org/10.2514/1.31083.

[8] M. Massari, F. Bernelli-Zazzera, Optimization of Low-thrust Trajectories for Formation Flying with Parallel Multiple Shooting, AIAA/AAS Astrodynamics Specialist Conference and Exhibit, Keystone, Colorado, 2006, https://doi.org/10.2514/6.2006-6747.

[9] G. Di Mauro, M. Lawn, R. Bevilacqua, Survey on guidance navigation and control requirements, J. Guid. Contr. Dynam. (2017), https://doi.org/10.2514/1.G002868.

[10] A.W. Koenig, T. Guffanti, S. D'Amico, New State Transition Matrices for Relative Motion of Spacecraft Formations in Perturbed Orbits, AIAA/AAS Astrodynamics Specialist Conference, SPACE Conference and Exposition, AIAA, 2016, https://doi.org/10.2514/6.2016-5635.

[11] K.T. Alfried, H. Yan, Evaluation and comparison of relative motion theories, J. Guid. Contr. Dynam. 28 (2) (2005) 254–261, https://doi.org/10.2514/1.6691.

[12] S. Sullivan, S. Grimberg, S. D'Amico, Comprehensive survey and assessment of spacecraft relative motion dynamics models, J. Guid. Contr. Dynam. 40 (8) (2017) 1837–1859, https://doi.org/10.2514/1.G002309.

[13] S. D'Amico, Autonomous Formation Flying in Low Earth Orbit, Ph.D. Dissertation, University of Delft, Delft, Netherlands, 2010.

[14] S. D'Amico, Relative Orbital Elements as Integration Constants of Hill's Equations, DLR-GNSOC TN 05-08, Oberpfaffenhofen, 2005.

[15] G. Gaias, J.-S. Ardaens, O. Montenbruck, Model of J2 perturbed satellite relative motion with time-varying differential drag, Celestial Mech. Dyn. Astron. (2015) 411–433, https://doi.org/10.1007/s10569-015-9643-2.

[16] J. Sullivan, A.W. Koening, S. D'Amico, Improved maneuver free approach angles-only navigation for Space rendezvous, Adv. Astronautical Sci. Spaceflight Mech. 158 (2016).

[17] C.W.T. Roscoe, J.J. Westphal, J.D. Griesbach, H. Schaub, Formation establishment and reconfiguration using differential elements in j2-perturbed orbits, J. Guid. Contr. Dynam. 38 (no. 9) (2015) 1725–1740, https://doi.org/10.2514/1.G000999.

[18] H. Schaub, J.L. Junkins, Analytical Mechanics of Space Systems, AIAA, Reston, Virginia (USA), 2014. Chap. 14.

[19] J. Crassidis, J.L. Junkins, Optimal Estimation of Dynamic Systems, CRC Press, 2004.

[20] J. Kiusalaas, Numerical Methods in Engineering with MATLAB, Cambrige University Press, 2005.

[21] K. Madsen, H.B. Nielsen, O. Tingleff, Methods for Non-linear Least Squares Problems, second ed., Informatics and Mathematical Modelling, Technical University of Denmark, DTU, 2004.

[22] J.J. More, The Levenberg-marquardt Algorithm: Implementation and Theory, vol. 630, Numerical Analysis, Notes in Mathematics (Springer Berlin Heidelberg), 1977, pp. 105–116, https://doi.org/10.1007/BFb0067700.

[23] D. Brouwer, Solution of the problem of artificial satellite theory without drag, Astronautical J. 64 (1274) (1959) 378–397.

[24] R. Lyddane, Small eccentricities or inclinations in the brouwer theory of the artificial satellite, Astron. J. 68 (8) (1963) 555–558.

[25] D. Vallado, Fundamentals of Astrodynamics and Applications, Springer-Verlag, New York, 2007.

[26] NASA, Small Spacecraft Technology State of the Art, 2015. NASA/TP–2015–216648/REV1.

[27] MathWorks, "MathWorks, Global Optimization Toolbox: User's Guide R2017a," The MathWorks, Inc., Natick, Massachusetts, United States.

[28] Z. Ugray, L. Lasdon, J. Plummer, F. Glover, J. Kelly, R. Marti, Scatter search and local NLP solvers: a multistart framework for global optimization, Inf. J. Comput. 19 (3) (2007) 328–340, https://doi.org/10.1287/ijoc.1060.0175.